OxyGen Electrochemical Air Purifier

![WPI logo]

A Major Qualifying Project Report

Submitted to the Faculty of the

WORCESTER POLYTECHNIC INSTITUTE

in partial fulfillment of the requirements for the

Degree of Bachelor of Science

in Chemical Engineering

Submitted by:

Connor Buek

Jacob Goodwin

Tyler Gundrum

May 13, 2021

Advisors: Ravindra Datta

Andrew Teixeira

Abstract

Millions of people every year require oxygen therapy for support or as life sustaining measures due to a rise in chronic illnesses and viruses, such as COVID-19, and the increase in the elderly population. The goal of this project was to design a unit that could efficiently and reliably produce a pure supply of oxygen, require low energy, and be environmentally friendly. This was achieved by developing a predictive OxyGen pump model and comparing it to literature data as well as producing further experimental data for support of the concept. In the end, while laboratory-based efforts to reproduce literature data were limited in success, a strong model for the data was produced that allowed for design specifications of the system to be calculated. Two final designs were created, one a mobile version for on-the-go usage and another that is more applicable to hospital-like settings, overall establishing a possible breakthrough in practical electrochemical oxygen production.

Table of Contents

Table of Figures

Table of Tables

Notation

$\Phi^o_{0,\rho}$	Standard equilibrium electrode potential
ΔG^o_r	Standard free Gibbs energy of reaction
ΔH^o_r	Standard change in enthalpy of reaction
ΔS^o_r	Standard change in entropy of reaction
σ_ρ	Coefficient for reaction
V	Potential for the cell (Voltage)
V^o_0	Standard equilibrium cell potential
T	Temperature
R	Universal gas constant
F	Faraday's constant
p_i	Partial pressure of species
p_A	Pressure of anode
p_C	Pressure of cathode
V_0	Equilibrium cell potential
$\Phi_{0,\rho}$	Equilibrium electrode potential
i	Current density
i_r	Current density supplied to electrode
V_{stack}	Potential supplied to entire system
N_{cell}	Number of cells in stack
$\beta^\bullet_\rho$	Symmetry factor on electrode
$v_{\rho,e-}$	Coefficient of electrons in electrode reaction
$i_{\rho,x}$	Crossover current density
$i_{\rho,o}$	Exchange current density
$i_{\rho,L}$	Limiting current density
L_{EL}	Length of membrane
σ_{EL}	Membrane conductivity
OCV	Open circuit voltage
$i_{\rho,r}$	Current density of reaction on electrode
$\eta_{r,\alpha}$	Overpotential on electrode
Q_r	Mass action term
a_i	Activity of species
T^o	Standard temperature
γ_M	Roughness factor
$i^*_{\rho,0}$	Intrinsic exchange current density
P_i	Permeance of species
c^o_i	Standard concentration of species
x_i	Mole fraction of species
η_B	Overpotential of membrane
n_i	Molar flow rate of species
v_o	Air volumetric flow rate
ORR	Oxygen reduction reaction
OER	Oxygen evolution reaction

HER   Hydrogen evolution reaction
HOR   Hydrogen oxidation reaction

1. Introduction

In the last decade, the need for personal oxygen supply has grown drastically given the ever-increasing rates of chronic illnesses, the continuous spread of viruses such as COVID-19, and an increasing elderly population. In fact, the worldwide market for personal oxygen concentrators, never mind personal oxygen tanks, hit one billion dollars in 2019 and is expected to grow to three billion by 2026 [1]. This growing reliance on oxygen suppliers not only begs for a more economical solution, but one that is also environmentally friendly, light-weight, and noiseless. The goal is to provide something to people that is not a daily reminder of the health problems they face but rather a convenient aid that could be used as needed.

Oxygen deficiency has been a cause of serious health issues for years, but now more so than ever people across the globe are in desperate need of oxygen for survival. Throughout 2020, the rapid spread of COVID-19 has caused devastating health effects and resulted in millions of deaths across the world. Being a respiratory disease in nature, it can cause dyspnea, or difficulty breathing, and prevent patients from being able to get enough oxygen to keep organs from failing. In June, when the pandemic was expanding at a rate of about 1 million new confirmed cases a week, the World Health Organization Director General, Tedros Adhanom Ghebreyesus, stated that about 620,000 cubic meters of oxygen per day were required to meet demand. That amount of oxygen would be enough to fill about 88,000 large oxygen tanks [2]. In order to treat respiratory illnesses such as this, oxygen therapy is necessary in order to prevent oxygen levels from dropping below the normal amount of 75 to 100 mmHg [3]. Furthermore, oxygen therapy is used to treat several illnesses or breathing disorders that prevent patients from being able to get enough oxygen on their own. Conditions such as chronic obstructive pulmonary disease, pneumonia, asthma,

bronchopulmonary disease, heart failure, cystic fibrosis, sleep apnea, lung disease, and trauma to the respiratory system can all prevent the lungs from absorbing enough oxygen. More than 1.5 million Americans currently require supplementary oxygen to maintain a regular quality of life due to these respiratory illnesses [3]. Additionally, patients with certain lung diseases and ones with higher oxygen needs are impacted to a greater degree than others because of physically unmanageable and inadequate portable systems [3]. Because of the especially high number of people with the need for supplemental oxygen across the globe, an increased access to small, lightweight, and easy to operate oxygen production systems is needed to optimize therapy for patients while also allowing them to live their normal lives.

To accomplish this goal, our team utilized a modified proton exchange membrane (PEM) electrolyzer to produce levels of high-grade purified oxygen that match the required purity and amount that meet oxygen therapy standards. Up until this point, PEM electrolyzers have been used largely to produce high grade hydrogen for commercial and industrial applications, most notably as a fuel production for hydrogen fuel cells, by splitting water into its base components of oxygen and hydrogen using electrochemistry. Water enters the electrolyzer at the anode where a catalyst and current carrying wire allows the water molecule to split into the hydrogen and oxygen ions. From there, the hydronium ions pass through a proton exchange membrane that promotes proton conductivity, allowing the ions to pass through to the cathode side of the cell. Here the hydronium ions combine into the base element hydrogen which is then discharged from the cell for collection with the oxygen being sent into the atmosphere. This modified plan intends to take advantage of the oxygen output by collecting it for the health-related needs of an individual. However, that still leaves behind the produced hydrogen in the outlet of the cathode. To resolve this part of the

problem, the cathode side of the cell would be consistently flooded with an oversupply of ambient air that will react with the adsorbed protons on the catalyst. This promotes two favored outcomes for a final design: reduced required power for electrolyzer operation and removes the potential hazard of disposing of highly reactive concentrated hydrogen into the surroundings.

The reaction between hydrogen and oxygen from air will cause an over potential on the cathode, depleting the driving force needed from the external power supply to electrolyze the water on the anode. Hydrogen in such conditions could ignite, injuring the user and damaging the electrolyzer itself. Although hydrogen itself is not harmful to breathe in, too much hydrogen production will displace the oxygen you breathe in, causing ill bodily function. This modified concept has been previously researched in a report from CSIRO Energy Technology published back in 2010 in which they found very promising initial data. Surprisingly enough, little to nothing has been conducted up until this point with the goal of furthering CSIRO's research. Upon further testing and design, this concept could be used to produce a constant supply of pure oxygen so long as the appropriate voltage and ambient air supply are always present. Once these parameters were optimized in our study of a single cell, the operations were scaled up to meet the required oxygen supply to help people in need of oxygen therapy. Scaling up PEM technology is a simple concept referred to as cell stacking where cells are stacked in parallel, and the power needed to supply the full system and the oxygen produced will be multiplied up from a single cell to the number of cells needed. This concept was explored for the final proposed solution that would ultimately meet current oxygen requirements of 0.5 to 5 liters per minute of oxygen depending on the person. This design will also be very environmentally friendly with the only waste from the system being reduced air. The end product goal was a unit that fits the pre-stated oxygen requirements, is

lightweight, easy to operate and maneuver with, and requires less power than current available methods.

2. Literature Review

2.1 Social Impacts

In terms of clinical use, a wide range of options currently exist to treat a shortage of oxygen. Compressed gas systems involve using a large stationary oxygen concentrator at home and a smaller portable oxygen tank to be taken outside the home [3]. The concentrator takes oxygen from the room, concentrates it for therapeutic use, and removes other naturally occurring gases. The concentrator itself is very difficult to move and can provide issues if the user wants a more portable option since portable oxygen tanks can be very limited in their capacity. Additionally, the oxygen supplied from this system is delivered in pulses, not continuously. Another option is using liquid oxygen instead of oxygen gas, which provides the benefit of being able to fit a larger amount of oxygen in a smaller tank due to the higher concentration [3]. Liquid oxygen must continuously be ordered for home delivery though, which leads to a higher financial burden. Additionally, liquid oxygen evaporates quickly and can be lost if not used in a timely manner. For more severe cases of respiratory complications, hyperbaric oxygen therapy becomes necessary. Hyperbaric oxygen therapy is a process in which patients are seated in a chamber where they are provided with 100% pure oxygen at a heightened pressure from a range of 2.0 to 2.5 atm's [4]. Patients are placed in one of two types of chambers; A monoplace chamber in which only one patient undergoes the process or a multiplace chamber that can hold multiple patients at once. Hyperbaric oxygen therapy is typically used for treatment of wounds, carbon monoxide poisoning, and clostridial gas gangrene [4]. With the exception of hyperbaric oxygen therapy, most treatment methods for respiratory complications are targeted at patients who have otherwise minimal health issues. Unfortunately,

current oxygen generation devices lack options for portable consumption over extended periods of time, preventing many patients from maintaining an active lifestyle.

On an industrial scale, oxygen is obtained through significantly different means. The two most common methods for industrial oxygen generation include cryogenic separation and pressure swing absorption. Cryogenic air separation is a process used to produce high purity oxygen or nitrogen at high volumes. Cryogenics is also the primary method by which liquid oxygen is produced. The idea behind the process is to lower the temperature of the air such that nitrogen and oxygen separate through distillation based on their boiling points, which occurs around -185 degrees Celsius [5]. If higher purity oxygen or liquid oxygen is required, further distillation is required. Cryogenic separation is most effective when either high purity oxygen is required (above, 99.5%), high volumes of oxygen are required (above 102 tons of oxygen per day), or high pressure oxygen is required [5]. Cryogenic air separators take more than an hour to start up, but are able to produce such a high purity of oxygen that the waste nitrogen stream is of a usable quality [5]. This can add significant financial benefits to separate processes integrated with cryogenic air separation. Pressure swing adsorbers, PSA, are a much newer technology as compared to cryogenic air separators. PSA devices take atmospheric air into a pressurized tank containing zeolites, which can deform and create a dipole under high pressures [5]. This dipole allows for the collection of nitrogen while allowing oxygen to pass. PSAs are generally kept at a minimum pressure of 1.5 atm's for the maximum oxygen enrichment. PSA devices are best suited for processes that do not require extremely high purities of oxygen (less than 95%). While PSAs can reach purities as high as 99.9%, the cost associated with going above 99.5% in a PSA device rises tremendously [5]. As

a result, PSA devices are best suited for small volumes of oxygen production, typically on the order of below 100 tons/day. As opposed to cryogenic air separators, which take up to an hour to start up, PSA devices only take a few minutes for start-up [5]. While both processes have their own benefits, an oxygen generation device capable of producing high purity oxygen without the financial burden of cryogenic requirements would be a useful addition for processes on an industrial scale.

2.2 Proton Exchange Membrane (PEM)

2.2.1 Fuel Cell

Fuel cells come in many configurations used for different commercial and industrial applications that provide high power density and have minimal environmental impact [6]. Proton Exchange Membrane Fuel Cells (PEMFC) are one such design and have been utilized today to supply power to stationary settings and portable applications, most notably transportation vehicles. This design is specific to these applications by performing at lower temperatures (50°C to 90°C) and pressures (1 atm to 5 atm) by utilizing potential differences of reactions across the working electrodes [7]. The lightweight and compact structure, high energy density output, environmental friendliness, and efficiencies have influenced the research and development of the systems for applications into today's society.

PEMFC's are composed of a membrane electrode assembly (MEA) packed between two bipolar plates, constructed of primarily graphite, on the two electrodes on opposite sides of the fuel cell, the cathode and anode, connected by a conducting wire providing power [8]. To fuel the cell, a stream of pure hydrogen gas enters the anode and a stream of oxygen, typically ambient or

pressurized air, enters the cathode. Once the hydrogen enters the cell, it flows through channels in the bipolar plate to uniformly distribute the hydrogen across the gas diffusion layer (GDL) to react with the catalyst in contact with it. This splits the hydrogen gas into two separate protons and carries the resulting free electrons across the bipolar plates and the current carrying wire to the cathode. The protons are then transported across the proton conductive membrane where it is adsorbed onto the catalyst on the cathode. Oxygen entering the cathode goes through channeling in the bipolar plates to uniformly distribute the gas across the diffusion layer to react with the protons on the catalyst and the transferred electrons from the current carrying wire to produce water. The transport of the protons and electrons are possible because of the potential difference of the electrochemical reactions that occur in the two electrodes. A model of this system can be seen in figure 2.1 with a table showing the reactions occurring with thermodynamic properties in table 2.1.
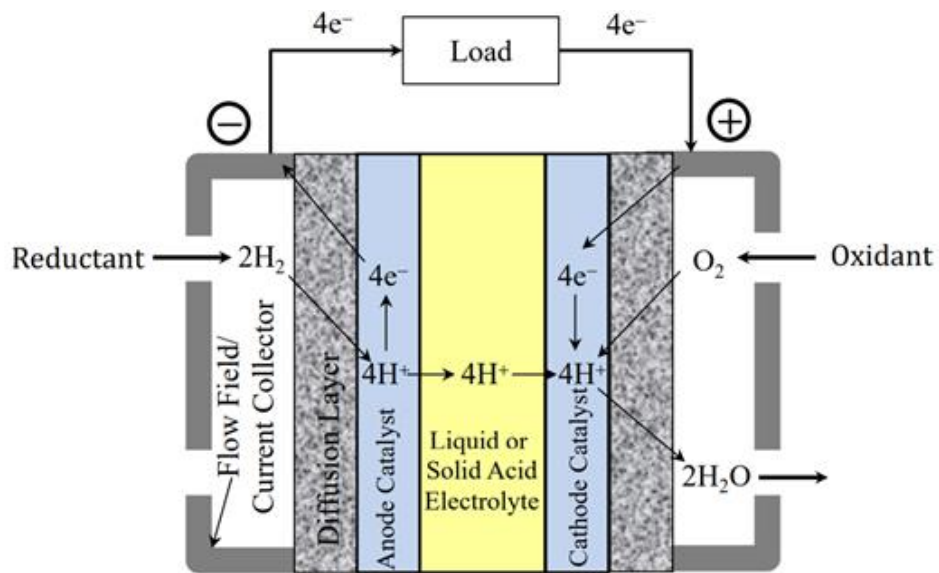
Figure 2.1: Model of a PEM Fuel Cell [8].

Table 2.1: Thermodynamic properties associated with each reaction occurring in a PEM Fuel Cell [8]

Electrode	Reaction, S_ρ	Potential (V)	ΔG_ρ^o (kJ/mol)	σ_ρ
Anode	$H_2 \rightleftarrows 2H^+$	$\Phi_{0,A} = 0$ V	0	+2
Cathode	$4H^+ + O_2 \rightleftarrows 2H_2O$	$\Phi_{0,C} = 1.229$ V	-474.3	+1
Overall	$2H_2 + O_2 \rightleftarrows 2H_2O$	1.229 V	-474.3 kJ/mol	$\Sigma\sigma_\rho S_\rho$

Material complications in the MEA and voltage losses from overpotentials in the electrode and membrane layers lead to some of the problems currently facing fuel cell application. The primary catalyst used in most fuel cells is platinum, which is either applied to the carbon paper gas diffusion layer or the membrane itself, typically Nafion. Platinum is a very rare metal and an expensive raw material, making PEMFC's expensive systems. It provides great adsorption for hydrogen to move the process forward but is prone to oxidation from oxygen in the cathode, leading to a decrease in the number of active sites and productivity. Metals such as iridium and rhodium have been applied to the cathode to prevent this process from occurring on the catalyst [9]. Productivity of the cell is also affected from the permeation of hydrogen across the membrane back to the anode. When this occurs, the system loses the potential from the electrochemical reaction the hydrogen participates in at the cathode. This is suppressed by increased membrane length and type of material [10].

Due to hydrogen crossover across the membrane and other thermodynamic losses affected by material properties, the open circuit voltage (OCV) or the voltage potential created by the fuel cell with an infinitesimally small current density, is less than the standard equilibrium potential described in table 1. The cell will typically operate around 1.0 V at OCV and will decline with an increase in current density supplied by the cell [11].

2.2.2 Electrolyzer

Purified hydrogen gas is a useful product to use in many commercial and industrial processes such as welding, hydrogenating fats and oils, cryogenics, production of methanol and hydrochloric acid, and hydrogen fuel cell operations [12]. Although hydrogen is the most abundant element in the universe, it is rare it exists in its diatomic hydrogen gaseous state as it is highly reactive with many compounds. Most processes that produce hydrogen gas are harmful toward the environment due to the large quantities of carbon dioxide that are released into the atmosphere. This includes practices such as gasification using coal and biomass and reforming natural gas, which consists mostly of methane [13]. A more environmentally friendly approach to produce high grade hydrogen is water electrolysis, where an external current is supplied to water from extra power generated from renewable sources that is not needed to power the grid, essentially breaking water down to its components of hydrogen and oxygen [14].

Proton exchange membrane water electrolysis (PEM-WE) uses the same technology and theories as described previously for PEMFC to produce high grade hydrogen gas to be used as a raw material or fuel for other applications. They are composed of an MEA loaded between two bipolar plates on the two electrodes connected by a current carrying wire which is supplied power from an external source [15]. To account for harsher operating conditions compared to the PEMFC potentials, the bipolar plates are made of titanium as opposed to graphite to reduce the oxidation that will occur in the anode, decreasing the productivity lost [11].

The operation of an electrolyzer is essentially a fuel cell run in reverse with an external power supply connecting the electrodes. Water is fed into the anode where it is dispersed across the gas diffusion layer and then broken down into protons and oxygen along the catalyst. The oxygen

retains the electrons from the reaction where it forms oxygen gas with another oxygen atom and is then pushed out through an outlet stream where it is released into the environment or collected to be used as high grade purified oxygen. Hydrogen protons are transferred across the proton conducting membrane from the anode to the cathode where it is adsorbed onto the catalyst. Electrons from the power supply are attached to the protons and hydrogen atoms combine to form diatomic hydrogen gas. The hydrogen is then diffused through the gas diffusion layer where it leaves as pure hydrogen out of the cathode. A model of this system can be seen in figure 2.2 with a table showing the reactions occurring in table 2.2.
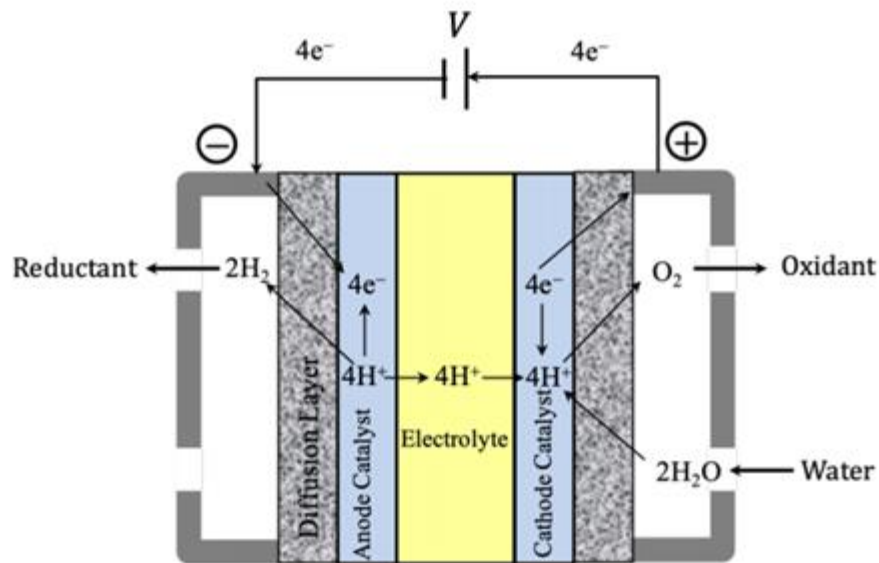
Figure 2.2: Model of a PEM Electrolyzer [15]

Table 2.2: Thermodynamic properties associated with each reaction occurring in a PEM Electrolyzer [8]

Electrode	Reaction, S_ρ	Potential (V)	ΔG_ρ^o (kJ/mol)	σ_ρ
Anode	$2H_2O \rightleftarrows 4H^+ + O_2$	$\Phi_{0,A} = 1.229$ V	474.3	+2
Cathode	$2H^+ \rightleftarrows H_2$	$\Phi_{0,C} = 0$ V	0	+1
Overall	$2H_2O \rightleftarrows 2H_2 + O_2$	-1.229 V	474.3 kJ/mol	$\Sigma \sigma_\rho S_\rho$

The overall process produces pure hydrogen and oxygen from the water fed into the system. However, overpotentials arise that deplete the productivity of the system, meaning that more power will need to be supplied compared to theoretical models to account for the overpotentials on the electrodes and membrane. Thermodynamic potentials to breakdown water into its components account for a large overpotential. The V_{max} is found using the enthalpy of formation rather than the free Gibbs energy of the reaction, which accounts for a higher voltage needed to break down the water ($\Delta H_{f,H20} > \Delta G_{f,H2O}$) [16]. The V_{max}, as described for fuel cells, requires more voltage for the electrolyzer system to operate, typically around 1.48 V operating at 25°C and 1.4 V at 80°C compared to 1.229 V for standard equilibrium potential. The gas crossover current density is another reason for the large overpotential at V_{max} [16]. Although membranes, such as Nafion, have been researched and developed to minimize crossover and promote proton conductivity, the V_{max} is significantly impacted. Materials used in the structure of the electrolyzer also account for losses. Permeation of hydrogen across the membrane back to the anode is dependent on the gas diffusion layer and membrane material, and this results in less hydrogen accumulated in the cathode steam. To produce the quantity of hydrogen needed, more power will need to be supplied to the electrolyzer to account for this phenomenon. One such system where this is a substantial factor is in asymmetric electrolyzers. Hydrogen needs to be pressurized in order to store properly and is

typically pressurized post-production which requires a lot of energy. Asymmetric electrolyzers have a pressurized cathode so the hydrogen is ready for storage after the electrolyzing step, bypassing the need to pressurize further. The differences in pressures across the electrodes initiates a lot of permeation and is typically subdued with larger membrane lengths [17]. As mentioned with PEMFC operations, the catalyst on the anode side must be modified to reduce oxidation occurring on a platinum catalyst. Iridium and rhodium are great to add to the catalyst to assist with the reduction of active sites over time [9]. The bipolar plates are operated with a harsher environment and increased voltage supplied to the electrodes as compared to PEMFCs, so titanium is substituted for graphite in order to decrease the amount of oxidation that occurs [18].

2.2.3 Membrane Electrode Assemblies

Membrane electrode assemblies (MEA) are at the heart of the traditional PEM fuel cell and electrolyzer and allow for the hydrogen or water decomposition reaction to occur fully without any unwanted by-products. A typical MEA consists of a proton exchange membrane (PEM) at the center, with a gas diffusion layer (GDL) on either side, typically made of a porous carbon cloth. A proton exchange membrane is a semipermeable polymer or composite surface constructed to conduct protons through it whilst acting as a barrier to oxygen and hydrogen gas. Very commonly composed of the fluoropolymer Nafion, it acts as the main divider between the cathode and anode sections of the electrolyzer. The gas diffusion layer is another type of barrier protecting the PEM. The layer is used as an electrical and thermal conductor between the membrane and electrode as well as a measure to prevent too much water from flooding the inner MEA whilst still allowing for consistent gas flow. The inner face of each GDL is coated with a specific catalyst for the anode

and cathode reactions. The catalysts' main purpose is to lower the activation energy on either side of the cell for the previously described reactions (section 2.2.2) to occur and therefore increases the electrochemical efficiency of the unit. This specific layout is known as a five-layer MEA and tends to be the most typical version used because of its low cost and high operation effectiveness. The five-layer is usually compared to both a three and seven layer MEA, all of which can be seen below in Figure 2.3.
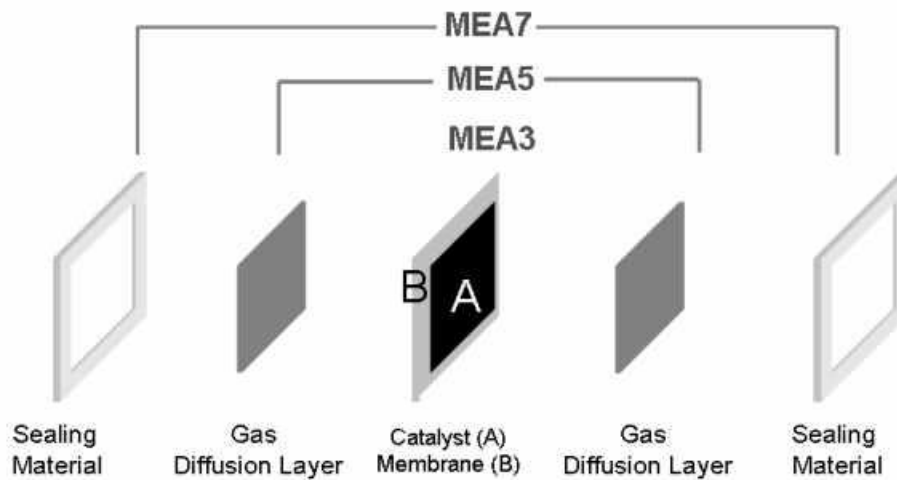
Figure 2.3: Composition of the different Membrane Electrode Assembly types. The MEA3 as depicted in the diagram above can also be referred to as a Catalyst Coated Membrane or CCM [19]

The three layer version simply consists of a PEM with a catalyst directly applied to either side of the membrane and is referred to as a Catalyst Coated Membrane (CCM). The reason that these CCMs do not come with gas diffusion layers on either side is simply for experimentation purposes so one can vary the compositional materials to determine what is best suited for their specific electrolyzer model. This piece alone plays greatly into the increased cost of a CCM because it is much harder to apply a catalyst directly on the membrane. The other relatively common version of an MEA is the seven layer. This is essentially a five-layer MEA with an external sealing material

on the outside edges of the GDLs on either side, typically made out of silicon and helps to improve the performance of the unit [19]. In the previously mentioned study conducted by CSIRO Energy Technology in 2009, a custom MEA was constructed in order to vary the catalysts used along with the amount loaded onto the GDL's. For the cathode side catalyst, 20 weight percent Pt/C was screen printed on the GDL made of porous carbon paper and the anode catalyst layer consisted of a thin layer of platinum deposited on titanium mesh with an additional Iridium Black surface coating. This was all hot pressed against a Nafion 115 proton exchange membrane. Out of all the catalyst variations attempted in this experiment including platinum, iridium, and rubidium, the aforementioned combination produced the best results with regards to "electrolysis voltage, catalyst loading, and long term stability"[16]. In an ideal scenario, the initial test for this report would have duplicated the MEA used here for reproducibility purposes as a baseline, however, it is extremely difficult to obtain membranes with the same exact catalyst loadings without custom MEA creation which is both expensive and very difficult. It has also been found that the majority of 5-layer MEA's available for purchase contain the same catalysts on either side of the membrane which is not optimal for our experiment. To combat this situation, a CCM loaded with $3mg/cm^2$ of Platinum black on the cathode side, and $3mg/cm^2$ of Iridium ruthenium oxide on the anode side was used [19]. However, this then means that GDL's still need to be added to the either side of CCM. It is very common for these layers to be made of a form of porous carbon paper simply due to its low cost. Given long periods of operation though, these layers can deteriorate and produce CO_2 due to oxidation on the anode side. Titanium mesh is a substitute that has proven to be successful in both enhancing the performance of the overall unit, along with taking much longer to deteriorate into TiO_2 [19]. Therefore, various configurations of each material including titanium

mesh for both sides, titanium on the anode side and carbon paper on the cathode side, and carbon paper on both sides will be used with the end goal of optimizing the production of oxygen.

2.2.4 Bipolar Plates

As previously described, two bipolar plates are contained within both a PEM-FC and a PEM-WE and have a wide range of functions for the unit. These include distributing reactants uniformly over the active areas, acting as a current conductor across the electrolyzer, preventing any leaking from the unit, and removing any heat buildup from the active area. An example of what paired bipolar plates look like can be seen below in Figure 2.4.
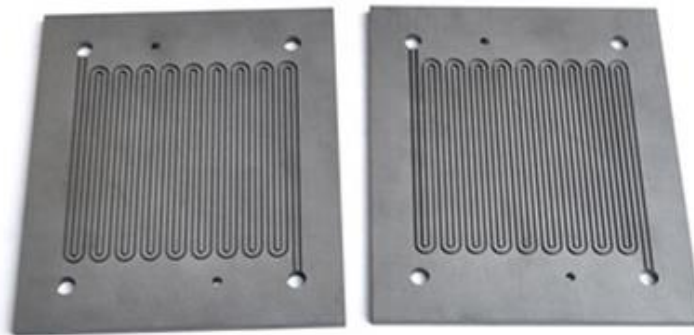
Figure 2.4: Graphite Bipolar Plates with a serpentine flow pattern [20].

The materials commonly used to make these plates are largely graphite, or some form of highly conductive metal such as titanium. There are many factors that play into identifying the optimal material to be used. Oxidation of the plates during consistent use is likely the most notable, specifically on the anode side of the cell where the plates are exposed to the oxygen evolution

reaction. This is largely why titanium plates are used as a substitute for a graphite plate even though graphite tends to cost less and still performs well in regards to low contact resistance and corrosion resistant properties [16]. Furthermore, given that the goal of this project is to produce some sort of stacked cell design to maximize the production of oxygen, means that graphite cannot be used for the final design. This is because in a stacked cell design, the plate is exposed to the anode of one cell and cathode of the next on either side. If the plate were graphite, this would ultimately cause degradation to occur of the cell over time, reducing its production levels and efficiency. Due to the low funding available for the project, graphite plates, similar to those in the pre-existing model, will be used. While this will not produce data that can be applied to a stacked cell to represent titanium plates, given that the experiment is short term and not running for drastically long periods of time, it will provide data that can be extrapolated for an entirely graphite cell stack.

2.2.5 Temperature and Pressure Dependence on PEM technology

As noted before, proton membrane exchange systems can operate at feasible temperatures and pressures as compared to other fuel cell and electrolyzer techniques such as solid oxide (500°C-1000°C), molten carbonate (650°C), and phosphoric acid fuel cells (150°C-250°C) [21]. Table 2.1 describes the standard equilibrium potential from the fuel cell operation, and is calculated when operated under standard temperature, 25°C, and pressure, 1 atm. From experimental results and fundamental thermodynamic principles determining the equilibrium cell potential from an increase in the temperature and pressure of the cell has shown to increase the system's productivity [22]. The equilibrium cell potential can be described using the Nernst Equation and entropic relationships by the equation below:

$$V_0 = V^o_{0,298} - \frac{\Delta S^o_{OR}}{\nu_{Ae^-} F}(T - 298) + \frac{RT}{\nu_{Ae^-} F} \ln \prod_{\substack{i=1 \\ i \neq e^-}}^{n} \left(a_i^{\nu_{Ai}}\right)\left(a_i^{\nu_{Ci}}\right) \qquad (2.1)$$

Where V_0 is the equilibrium potential across the cell given temperatures and species activities, $V^o_{0,298}$ is the standard equilibrium potential at 298 K, ν_{Ae^-} is the coefficient of the electron transfer for the reaction describing the whole cell, and $a_i^{\nu_{Ai}}$ and $a_i^{\nu_{Ai}}$ are the activities of the species on the anode and the cathode respectively. As temperature increases, so will V_0 and although the pressure increase will not have a large effect on the partial pressures of hydrogen and oxygen in the anode and cathode respectively, the partial pressure of water produced in the cathode will decrease as a result of the Antoine equation, forcing more water to remain in the liquid form [23]. This effect will increase the cell's equilibrium potential as described in equation 2.1. Both parameters have been experimented on at Mississippi State University and the Babol Noshirvani University of Technology (NIT), showing parallel results:
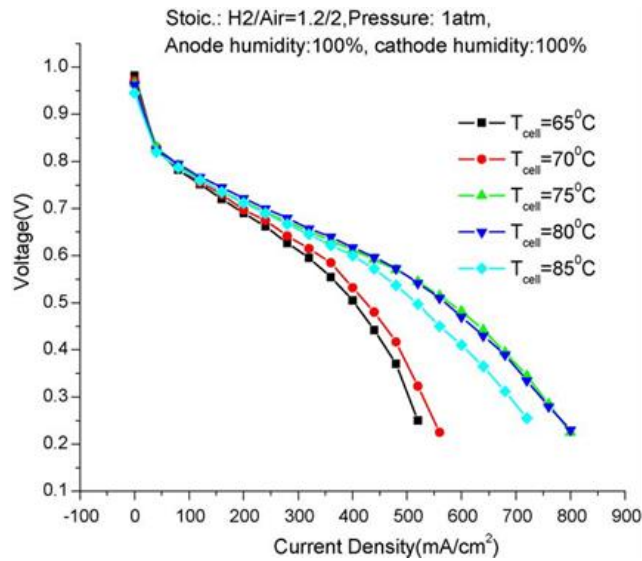
Figure 2.5. Cell voltage dependence on temperature [22].
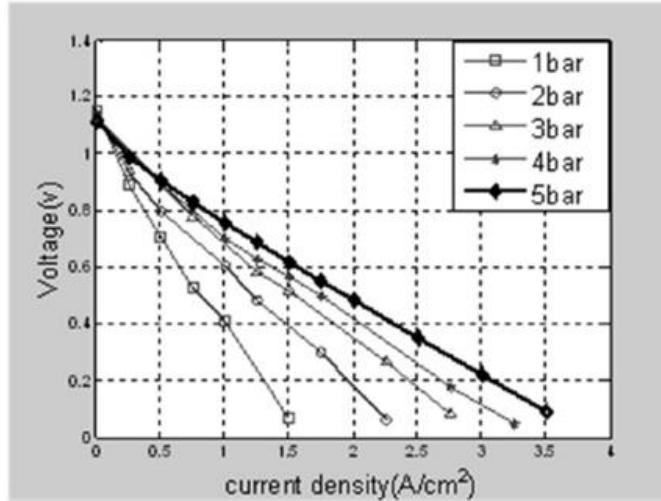
Figure 2.6. Cell voltage dependence on pressure [24].

It is important to note that the experiments conducted will be using deionized liquid water, so the temperature and pressure used will not cause the water to evaporate inside the cell. This causes complications in gas crossover current of water and blocking active sites on the anode for electrolyzers and cathode for fuel cells [15]. It will also increase the standard equilibrium cell potential as the thermodynamic laws for liquid water and gaseous water are different.

2.2.6 Industrial and Commercial Uses

PEM fuel cells and electrolyzers are used in many applications in industrial and commercial practices. One of the more prominent fields fuel cells have been researched is for feasibility in automobiles and other vehicles, as PEM technology allows for standard operating conditions [21]. Toyota, Honda, General Motors, and other companies have been experimenting with fuel cell powered cars, essentially rendering the automobiles as electric vehicles [19]. However, instead of being powered by a heavy lithium ion battery as seen in Tesla models, these vehicles are powered by a high energy density PEM fuel cell, fueled by a stream of high purity hydrogen from a tank.

27

For PEM fuel cells to be capable of powering automobiles and other devices requiring high power outputs, stacking multiple cells together becomes necessary. According to the equation:

$$V_{Stack} = N_{Cell}(V) \qquad (2.2)$$

Stacking multiple cells together directly increases the total fuel cell voltage proportionally to the number of cells in the stack. Essentially, a higher amount of hydrogen and a higher power supply can be produced by increasing the number of cells, which allows for the powering of automobiles to become feasible. Beyond just automobiles though, fuel cells in general have been becoming more prominent in a number of other applications including scooters and bicycles, utility vehicles such as forklifts, small fuel cell based power systems for homes, backup power generators for telecommunicators, miniature fuel cells for portable battery replacements for electronic devices such as cellphones, and even space orbiters for the U.S. space program [25]. Additionally, electrolyzers can also be used to store energy for future use. This is done by storing small amounts of hydrogen produced from electrolysis in pressurized vessels or solid metal hydrides [25]. Underground salt caverns can also be used to store much larger amounts of hydrogen. This stored hydrogen can then be re-electrified in fuel cells with efficiencies up to 50% [25], essentially allowing for energy storage of capacities much higher than batteries normally allow for.

2.3 Modeling Cell Polarization

To investigate the potential needed for a PEM electrolyzer and output from a PEM fuel cell, the equilibrium potential and losses across the anode, cathode, membrane, and gas diffusion layer are

accounted for. This allows researchers to see how well experimental systems match with theoretical potential at specific current densities. It is useful in determining specific operating conditions to run a cell at as well as determining which materials would maximize the productivity for the system. To account for all thermodynamic and material overpotentials, the following equation is used to predict the potential based on the current density of a fuel cell:

$$V = V_0 - \frac{RT}{\beta_A^\bullet v_{Ae^-}^\bullet F} \sinh^{-1}\left\{\frac{1}{2}\left(\frac{i/i_{A,0}}{1-i/i_{A,L}}\right)\right\} + \frac{RT}{\beta_C^\bullet v_{Ce^-}^\bullet F} \sinh^{-1}\left\{\frac{1}{2}\left(\frac{(i+i_{C,X})/i_{C,0}}{1-(i+i_{C,X})/i_{C,L}}\right)\right\} - i\left(\frac{L_{EL}}{\sigma_{EL}}\right) - i(R_I) \qquad (2.3)$$

Where V_0 is the equilibrium potential, found in equation (2.1), R is the universal gas constant, T is the temperature the cell is operating at, $B_A^\bullet$ is the symmetry factor, v_{Ae^-} is the reaction coefficient for electron transportation between the electrodes, i is the current density of the cell, $i_{A,0}$ and $i_{C,0}$ are the exchange current density of the anode and cathode respectively, $i_{A,L}$ and $i_{C,L}$ are the limiting current densities of the anode and cathode respectively, $i_{C,X}$ is the crossover current density of the cell, L_{EL} is the length of the membrane used, and σ_{EL} is the proton conductivity of the membrane. The exchange and limiting current densities of the electrodes are heavily dependent on the catalyst and electrode materials used. A significant contribution to the overpotentials of the cell are due to the electrodes containing oxygen — the cathode for fuel cells and anode for electrolyzers — due to the oxygen reduction reaction (ORR) and the oxygen evolution reaction (OER) because of oxygen poor adsorption properties compared to hydrogen and the water presence in both systems that block active sites on the catalyst layer [8]. From the equation above, these overpotentials are seen to be more dominant as current density increases, and this is backed by experimental polarization curves.

Electrolyzers follow the same model as fuel cells, the only difference being that the signs of the components in the equation are flipped, so instead of cell potential decreasing with current density in the cell, the potential will instead increase. Again, this is backed by experimental polarization curves for electrolyzer operations [8]. Polarization curves for fuel cells and electrolyzers are made from the equation describing the overpotentials in the electrodes and the membrane shown in figure 2.7.
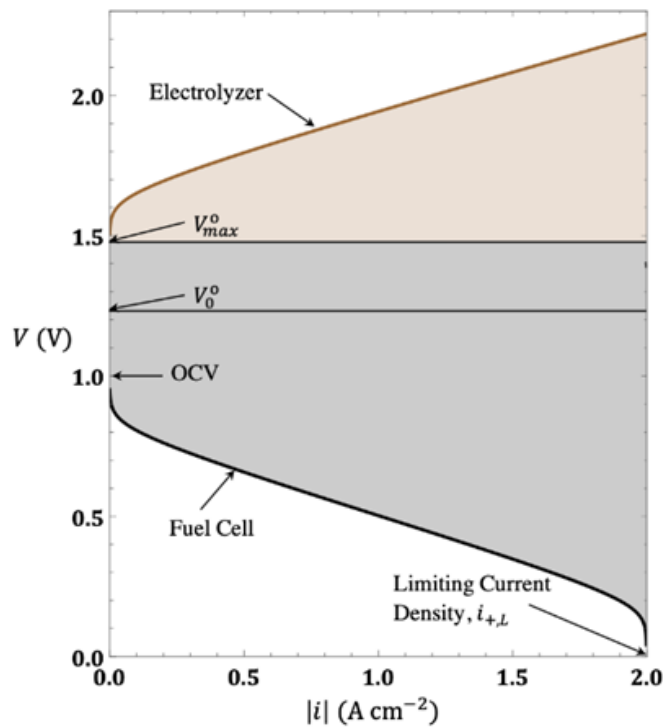
Figure 2.7. Polarization curve for fuel cell and electrolyzer operations [15]

2.4 Oxygen Pumps

With portable oxygen currently being in large demand due to both medical and analytical purposes, the most common method for obtaining it currently is through absorption oxygen concentrators from air. This method poses the problem though of also potentially concentrating harmful mixtures

from air. Additionally, oxygen can be obtained through water electrolyzers, though this method has the drawback of requiring high energy consumption due to the high potential of the ORR and OER reactions. Electrochemical oxygen pumps seek to partly compensate for this potential by the depolarization of the cathode through delivery of air from the atmosphere into the cathode. In this case, the following electrochemical reactions occur in the cathode and anode catalytic layers of a cell:

$$\text{cathode: } O_2 + 4H^+ + 4e \rightarrow 2H_2O,$$
$$\text{anode: } 2H_2O \rightarrow O_2 + 4H^+ + 4e.$$
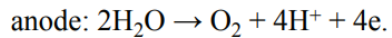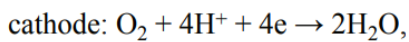
If the difference between the partial pressures of oxygen in the anode and cathode chambers is disregarded, the equilibrium voltage of the cell is 0 V, although there are several problems affecting the efficiency of the process in practice. One of the important problems is achieving optimal water balance of the cathode catalytic layer because its watering leads to screening of the catalyst surface. On the other hand, a lack of enough water leads to an increase in the ohmic loss in the layer and in the cell as a whole [26]. The current development of electrochemical oxygen pumps is primarily aimed to use the configurations of standard fuel cells or electrolysis cells.

Experimental research previously performed in a laboratory cell with a solid polymer electrolyte demonstrated that raising the air flow rate to 1.5 liters per minute at atmospheric pressure improves the efficiency of the cathode process because of the more effective removal of the excess of water from the carbon current collector and catalytic layer, and leads to an increase in the oxygen concentration in the layer [26]. However, raising the air flow rate much further, up to 4 liters per minute at a current density of 1.0 A/cm^2 hardly affects the cell parameters [26]. This is likely due to steady conditions being reached for the mass-transfer processes in the catalytic layer.
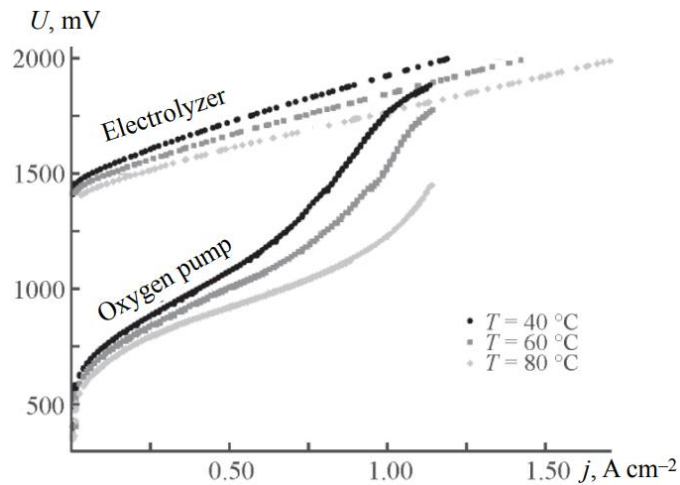
Figure 2.8. Voltage-Current Characteristics of a Cell in Electrolyzer and Electrochemical Oxygen Pump

Modes [26].

The polarization characteristics of the laboratory cell with a solid polymer electrolyte, operating in both the electrolyzer and electrochemical oxygen pump modes, are shown in Figure 2.8. The effect of temperature in the case of electrolysis is primarily due to the decrease in the overpotential of the cathodic and anodic reactions and to the lower membrane resistance. It is worth noting that the U(I) characteristic of the laboratory cell operating in the oxygen pump mode has several characteristic regions. The first two are also characteristic of the operation of the electrolysis cell; As the current density increases, a gradual transition is observed from the range in which the overpotential of electrode reactions plays a dominant role to the rise in voltage. The further increase in voltage at current densities exceeding 0.5 amps per centimeter squared is likely due to the diffusion limitation associated with the transport of oxygen and with the fall of its concentration in the cathode catalytic layer [26]. This is indirectly confirmed considering that raising the air pressure leads to an insignificant rise in current density, and raising the temperature as shown in

Figure 2.8 moves this rise in voltage toward higher current densities. As the current density increases further, the electrochemical oxygen pump characteristics become comparable to those of the electrolysis cell.
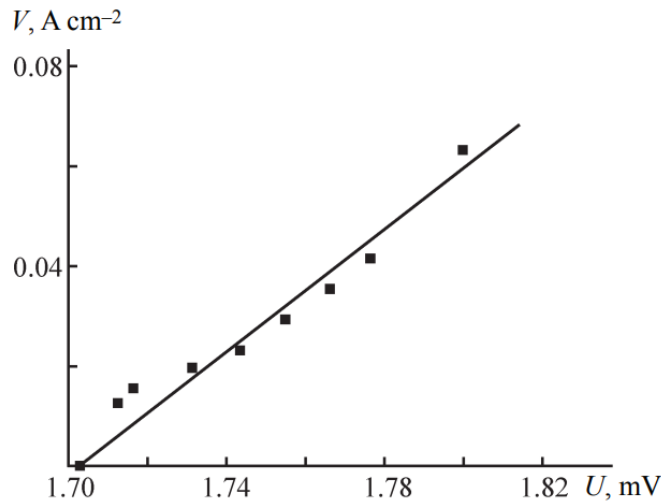
Figure 2.9. Hydrogen Evolution Rate in the Cathode Catalytic Layer Versus the Voltage in the Electrochemical Oxygen Pump Mode [26].

It is worth noting that, at voltages of less than 1.23 volts on the electrochemical oxygen pump cell at about 1 A/cm^2 and 80 degrees Celsius, no hydrogen was found in air outflowing from the cathode compartment [26], and only small amounts of hydrogen were detected at voltages exceeding 1.7 Volts as shown in figure 2.9. At a voltage of 1.8 V, the content of hydrogen in air reached a value of 0.25 vol % [26]. The rate of hydrogen evolution in the cathode carbon layer, shown in figure 2.9, at cell voltages in the range 1.7–1.8 V is more than an order of magnitude lower than rate that would be observed in the electrolysis mode, although the U(I) characteristics of the electrolysis cell and electrochemical oxygen pump nearly the same in this range of potentials [26]. It can be assumed in this case that, passing across the catalytic layer, atmospheric oxygen reacts with hydrogen on the catalytic surface, but has not had enough time to react with hydrogen

ions due to the screening of the catalyst surface by water (the flow of water with hydroxonium ions grows with increasing current density) [26]. This suggests that further optimization of the mass-transfer processes and the water balance of the carbon layer would enable use of the cell in the electrochemical oxygen pump mode also at high current densities. The process of the electrochemical concentration of oxygen from air also remains safe at current densities exceeding 1 A/cm^2. Overall, electrochemical oxygen pumps have the potential to significantly reduce the high energy expenditure of water electrolyzers to become an efficient method of oxygen production with further optimization. To determine the parameters of how an oxygen pump could be optimized to the point of being able to compete with currently used methods of oxygen provision, a model was created that would demonstrate the potential oxygen outputs and power requirements of an electrochemical oxygen pump system.

3. OxyGen Pump Modeling

The primary purpose of proton exchange membrane water electrolysis (PEM-WE) is to create a steady output of pure hydrogen to be used as fuel or for industrial production by electrolyzing water fed into the anode (positive electrode). The OxyGen model utilizes similar practices, however a steady stream of air is supplied to the cathode (negative electrode) to react with protons and electrons transferred from the anode to form water, reducing the potential of the cathode while the anode outputs high purity oxygen on demand [15]. An external power supply is needed to transfer electrons from the anode, where the electrons are produced, to the cathode where they are consumed. The current density (i) is defined as the flow of the protons, or positive charges, flowing in the opposite direction. Figure 3.1 depicts a single cell of the OxyGen model setup.
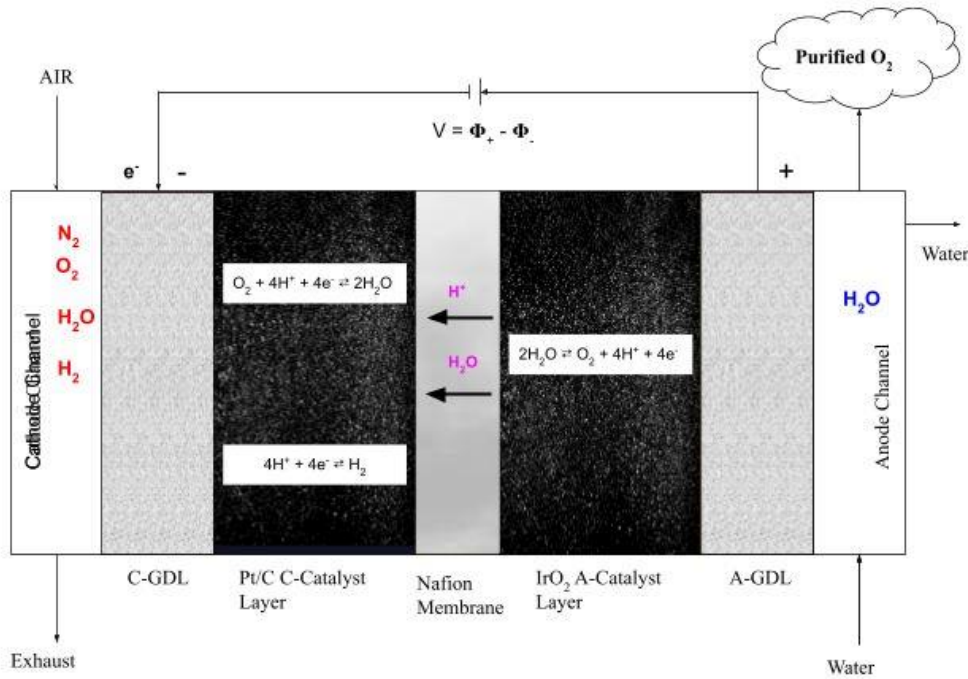
Figure 3.1. Schematic of OxyGen Air Purifier Single Cell

The cathode is composed of a serpentine graphite delivery channel (bipolar plate), carbon paper to act as the gas diffusion layer (GDL), and a Pt/C catalyst. The anode bipolar plate was identical to

the cathode while its GDL was a titanium mesh screen with an $IrRuO_2$ catalyst layer. The harsher conditions, sluggish nature of the oxygen evolution reaction (OER), and tendency towards carbon oxidation on the positive electrode highly influenced the decision to use these materials for effective cell operation. To complete the membrane electrode assembly (MEA) is the polymer membrane composed of Nafion 115, sandwiched between both electrodes. The model being tested will have an active area of 50 cm^2.

3.1 Reactions

At lower values of i and lower voltages (V→0), the oxygen reduction reaction (ORR) will occur on the cathode due to larger irreversibilities compared to the hydrogen evolution reaction (HER). The standard equilibrium potential for each electrode is determined from the standard equilibrium free Gibbs energy from the reaction given the relationship:

$$\Phi^o_{\rho,0} = \frac{\Delta G^o_{\rho,0}}{\nu_{\rho,e-} * F}$$

(3.1)

Where $\Phi^o_{\rho,0}$ is the standard equilibrium for electrode ρ, $\Delta G^o_{\rho,0}$ is the standard equilibrium free Gibbs energy for the reaction in the electrode ρ, $\nu_{\rho,e-}$ is the coefficient for electrons in the reaction for electrode ρ, and F is Faraday's constant. For such conditions, the reactions on both the anode and cathode can be seen below:

Table 3.1. ORR Reaction Table: OxyGen reactions. Potential of the cell is given by the difference of the reaction potential on the Anode and the reaction potential on the Cathode ($\Phi^o_{+,0}$ - $\Phi^o_{-,0}$). The free Gibbs energy of the entire cell is given as the summation of the free Gibbs energy of the reactions occurring on the Anode and the Cathode.

Electrode	Reaction, s_r	Potential (V)	$\Delta G^o_{r,0}$ (kJ mol^{-1})
Cathode:	$O_2 + 4H^+ + 4e^- \rightleftarrows 2H_2O$	$\Phi^o_{-,0} = 1.229$	-474.4
Anode:	$2H_2O \rightleftarrows O_2 + 4H^+ + 4e^-$	$\Phi^o_{+,0} = 1.229$	474.4
Cell	$O_{2,-} \rightleftarrows O_{2,+}$	$V^o_0 = 0$ V	0

The reactions occurring on the two electrodes are identical in the reverse reaction to one another, making the standard equilibrium potential for the cell, V^o_0, zero. As mentioned before, an external power source will be needed to drive electrons from the anode to the cathode to deliver electrons because of inefficiencies in the cell that create overpotentials. This will be described later in the report.

At higher voltages and current densities ($i > i_{-,L}$), the oxygen concentration in contact with the catalyst on the cathode approaches zero. When this happens and the voltage supplied to the cell still increases, transferring more electrons to the cathode, the HER becomes kinetically favorable thereby producing hydrogen gas in the cathode. For the purposes of the OxyGen model, the HER reaction is unfavorable, as the standard equilibrium potential for the cathode is decreased significantly during HER operations, meaning even more voltage (or power costing energy and capital) will need to be supplied to the cell for anymore current and purified oxygen to be produced compared to just the ORR occurring. Table 3.2 shows the HER reaction below. It should be noted that the ORR and HER will be occurring simultaneously with such conditions, but the polarization of the cell will be commanded by the unfavorable HER.

Table 3.2. HER Reaction Table: PEM-WE reactions. Potential of the cell is given by the difference of the reaction potential on the Anode and the reaction potential on the Cathode ($\Phi^o_{+,0}$ - $\Phi^o_{-,0}$). The free Gibbs energy of the entire cell is given as the summation of the free Gibbs energy of the reactions occurring on the Anode and the Cathode.

Electrode	Reaction, s_r	Potential (V)	$\Delta G^o_{r,0}$ (kJ mol^{-1})
Cathode:	$4H^+ + 4e^- \rightleftarrows 2H_2$	$\Phi^o_{-,0} = 0$	0
Anode:	$2H_2O \rightleftarrows O_2 + 4H^+ + 4e^-$	$\Phi^o_{+,0} = 1.229$	474.4
Cell	$2H_2O \rightleftarrows O_2 + 2H_2$	$V^o_0 = 1.229$ V	474.4 kJ mol^{-1}

A transition point occurs once the current density surpasses the limiting current density of the cathode. Diffusion limitations of the oxygen through the GDL to react with the protons transferred from the OER on the anode create stoichiometric limitations in the ORR. The current density supplied to the cathode will be fully consumed in the ORR so long as it does not surpass the limiting current density. As mentioned before, it is more favorable in lower voltage conditions:

$$i_- = i_{-,ORR} \qquad (i_- < i_{-,L}) \qquad (3.2)$$

When the current density of the cathode does surpass the limiting current density, the HER occurs and the remaining proton transfer will supply the reaction. This can be described as:

$$i_- = i_{-,ORR} + i_{-,HER} \qquad (i_- > i_{-,L}, \, i_{-,ORR} = i_{-,L}) \qquad (3.3)$$

There will no longer be a standard equilibrium potential on the cathode while the HER occurs, leading to an abrupt change in the polarization curve. This was depicted in an experiment performed at CSIRO Energy Technology in Victoria, Australia [16]:
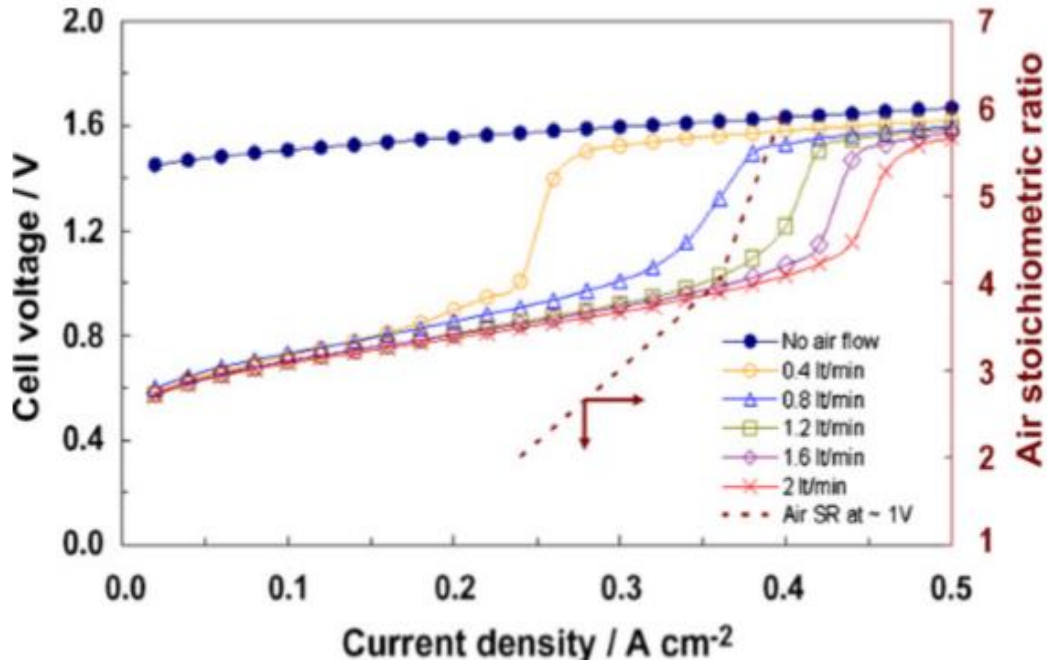
Figure 3.2. Polarization curve varying cathodic air flow and stoichiometric ratio [16].

This experiment depicted the transition point well along with the overpotentials of the cathode once the limiting current density was reached. As anticipated, the transition was quite abrupt and stabilized operating as a "normal electrolyzer" or when no air flow was presented to the cathode. The polarization at each airflow was compared to normal electrolyzer operations and a large difference was seen when the HER had yet to begin due to the lack of overpotential resisting the transfer of electrons. Once the HER started, the graph displayed a small difference between normal operations and when there was air supplied. This is because the current density supplying the HER begins once the transition point is surpassed, meaning the polarization will sharply increase to the equilibrium potential of the HER, 1.229 V, and then increase at the rate of a normal electrolyzer instead of starting at that range when the current density of the cell is 0. This can be explained by the rationale for equation 3.2.

Another obvious point to be made from the data collected is the difference between the air flow rates in the cathode. The transition point occurred at later current densities for larger air flows. This is because with more air entering the cathode, more oxygen can diffuse through the GDL and can react more with the protons transferring at higher current densities, thereby increasing the limiting current density of the cathode. This is also described later in the paper.

3.2 Theory

The OxyGen purifier model has a standard equilibrium potential of zero between the two electrodes as mentioned before, but an external power source was still needed to drive electrons to the cathode due to overpotentials in both electrodes described here. These overpotentials are caused by some inefficiencies in the cell, due to diffusion limitations, exchange properties, and material properties. At the electrodes, this overpotential can be described as:

$$\eta_{r,\alpha} = \Phi_\alpha - \Phi_{r,0} \tag{3.4}$$

Where $\eta_{r,\alpha}$ is the overpotential contribution of an electrode, Φ_α is the potential of the electrode, and $\Phi_{r,0}$ is the equilibrium electrode potential (different from the standard equilibrium electrode potential as it is described using the Nernst Equation to describe the operational temperature). The Nernst equation given in equation 3.5 gives the equilibrium electrode potential for any operating temperature and species composition:

$$\Phi_{r,0} = \Phi_{r,0}^o + \left(\frac{RT}{v_{re-}F}\right) \ln Q_r \tag{3.5}$$

Where Q_r describes the mass action terms of the species activities:

$$Q_r = \prod_{i=1}^{n} a_i^{\nu_{ri}} \tag{3.6}$$

and the standard equilibrium electrode potential, $\Phi_{r,0}^o$, is described above in equation 3.1. This would be the electrode potential at the standard temperature, unit species activity equal to 1, meaning a pure species, or gases at a pressure of 1 atm.

The Gibbs free energy of a reaction is also a function of temperature, affecting the standard equilibrium potential. To solve for this potential, the relation of the standard enthalpy and entropy change to find temperature dependence was used seen below:

$$\Delta G_r^o = \Delta H_r^o - T\Delta S_r^o \tag{3.7}$$

Substituting potential terms to solve for the standard equilibrium potential at a given temperature, equation 3.8 is produced.

$$\Phi_{r,0}^o = \Phi_{r,0,T^o}^o - \frac{\Delta S_r^o}{\nu_{re-}F}(T - T^o) \tag{3.8}$$

The Nernst equation described in equation 3.5 can now be put together to form:

$$\Phi_{r,0} = \Phi_{r,0,T^o}^o - \frac{\Delta S_r^o}{\nu_{re-}F}(T - T^o) + \left(\frac{RT}{\nu_{re-}F}\right)\ln \prod_{i=1}^{n} a_i^{\nu_{ri}} \tag{3.9}$$

Represented here are the equilibrium electrode potential equations which relate the equilibrium potentials at each electrode for the reactions in the cell:

Anode OER equilibrium potential

$$H_2O \rightleftharpoons 1/2O_2 + 2H^+ + 2e^-$$
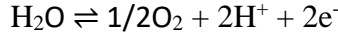
$$\Phi_{OER,+,0} = \Phi^o_{OER,+,0,T^o} - 8.46x10^{-4}(T - 298K) + \left(\frac{RT}{3F}\right)\ln\frac{\alpha^2_{H^+}\left(p_{O_2}/p_+\right)^{1/2}}{a_{H_2O}} \qquad (3.10)$$

Where p_+ is the total pressure of the anode.

Cathode ORR equilibrium potential

$$1/2O_2 + 2H^+ + 2e^- \rightleftharpoons H_2O$$
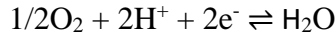
$$\Phi_{ORR,-,0} = \Phi^o_{ORR,-,0,T^o} - 8.46x10^{-4}(T - 298K) + \left(\frac{RT}{-2F}\right)\ln\frac{a_{H_2O}}{\alpha^2_{H^+}\left(p_{O_2}/p_+\right)^{1/2}} \qquad (3.11)$$

Where p_- is the total pressure of the cathode.

Cathode HER equilibrium potential

$$2H^+ + 2e^- \rightleftharpoons H_2$$

$$\Phi_{ORR,-,0} = \Phi^o_{ORR,-,0,T^o} - 8.46x10^{-4}(T - 298K) + \left(\frac{RT}{-2F}\right)\ln\frac{p_{H_2}/p_-}{\alpha^2_{H^+}} \qquad (3.12)$$

Assuming cell operation at lower current densities and voltages, these equations can be combined to produce the potential difference between the electrodes for the entire cell using the relationship:

$$V_{cell,0} = \frac{RT}{4F}\ln\left(\frac{p_-}{p_{O_2,-}}\right)\left(\frac{p_{O_s,+}}{p_+}\right) \qquad (3.13)$$

The vapor pressure of water in both electrodes has an impact on the partial pressure of the oxygen and hydrogen in the same channels, affecting the cathode more than the anode. At lower operating temperatures, this can lead to a significant impact. The vapor pressure of water is found using the Antoine equation described in atm, using temperatures in degrees kelvin:

$$\ln p^o_{H_2O} = A - \frac{B}{T + C} \tag{3.14}$$

where A = 11.676, B = 3816.44, and C = -46.13.

The current density for each electrode can be found from the Butler-Volmer equation relating species composition and overpotential:

$$i_r = i_{r,0}\left[\exp\left(\frac{\overrightarrow{\alpha_r}F\eta_{r,\alpha}}{RT}\right) - \exp\left(-\frac{\overleftarrow{\alpha_r}F\eta_{r,\alpha}}{RT}\right)\right] \ (A \ cm^{-2} \ MEA) \tag{3.15}$$

The activity of a reaction, α_r, is described using the relationship:

$$\overrightarrow{\alpha_r} = \beta_\rho^{\cdot}\nu^{\cdot}_{\rho,e-} \ ; \ \overleftarrow{\alpha_r} = (1 - \beta_\rho^{\cdot})\nu^{\cdot}_{\rho,e-} \tag{3.16}$$

Where $\nu^{\cdot}_{\rho,e-}$ is the coefficient of electrons in the rate determining step (RDS) of the electrode overall reaction and $\beta_\rho^{\cdot}$ is the symmetry factor, usually assumed to be ½.

The exchange current density of an electrode describes the feasibility an electrode must proceed with the reaction. This can be seen as the amount of active site available on the catalyst and electrochemical environment provided by the cell. The exchange current density, $i_{r,0}$, can be found using the equation:

$$i_{r,0} = \gamma_M i^*_{r,0} \tag{3.17}$$

where γ_M is the surface roughness described as the amount of catalyst per area MEA, and $i^*_{r,0}$ is the intrinsic exchange current density.

To account for the diffusion limitations of the reactants diffusing through the GDL because of material properties and species activities, the limiting current density was added to the equation. The limiting current density describing the species on an electrode can be found:

$$i_{r,L} = n(P_i)Fc_i^o a_{i,b} \qquad (3.18)$$

where n is the coefficient of the limiting species of the electrode reaction, P_i is the permeance of the species (describing the mass transfer of the species), c_i^o is a standard concentration of the species, and $a_{i,b}$ is the species activity in the bulk concentration. The activity of the proton transfer and liquid water in the anode are assumed to be unit activity ($a_{H^+} = a_{H_2O(l),+} = 1$). The activity of the oxygen, hydrogen and water vapor is described from the partial pressures, or molar composition, assuming ideal gases. The activities are found by $a_{H_2} = x_{H_2}$, $a_{O_2} = x_{O_2}$, and $a_{H_2O} = x_{H_2O}$.

The limiting current density is then added to the Butler-Volmer equation as:

$$i_r = i_{r,0}\left(1 - \frac{i_r}{i_{r,L}}\right)\left[\exp\left(\frac{\overrightarrow{a_r}F\eta_{r,\alpha}}{RT}\right) - \exp\left(-\frac{\overleftarrow{a_r}F\eta_{r,\alpha}}{RT}\right)\right] (A\ cm^{-2}\ ECSA) \qquad (3.19)$$

where ECSA is the electrochemical surface area. To simplify further, it can be assumed $\overrightarrow{a_r} = \overleftarrow{a_r} = a_r$ and arrange the equation as:

$$\frac{i_r/i_{r,0}}{1 - i_r/i_{r,L}} = 2\sinh\left(\frac{a_r F\eta_{r,\alpha}}{RT}\right) \qquad (3.20)$$

This expression can then be rearranged to find the overpotential at the electrodes:

$$\eta_{r,\alpha} = \left(\frac{RT}{a_r F}\right)\sinh^{-1}\left[\frac{1}{2}\left(\frac{i_r/i_{r,0}}{1 - i_r/i_{r,L}}\right)\right] \qquad (3.21)$$

This expression directly quantifies the overpotential at an electrode based on the kinetic and diffusive properties. Equation 3.21 was used to describe the overpotentials in the polarization equation for both electrodes. The positive electrode experienced very little diffusion limitations as it had a constant stream of water to readily react with the catalyst. The limiting current density was very large ($i_r \ll i_{r,L}$) so it was therefore reasonable to simplify the expression for the OER on the anode to:

$$\eta_{OER,+} = \left(\frac{RT}{\alpha_{OER}F}\right)\sinh^{-1}\left[\frac{1}{2}\left(\frac{i_r}{i_{r,0}}\right)\right] \tag{3.22}$$

The potential of the cell is equal to the sum of all the overpotentials of the system in series. When there was no current supplied to the system, the potential just equaled the equilibrium potential ($V = V_0$). The polarization model can be shown as:

$$V = V_0 + \eta_+ - \eta_- + \eta_B + \eta_I \tag{3.23}$$

where η_B is the inefficiency due to potential lost in the membrane and η_I is the correction term for the interfacial resistances. For simplicity's sake, the interfacial resistances will be neglected when evaluating the polarization of the model. The expression for the membrane overpotential is:

$$\eta_B = i_B \left(\frac{L_B}{\sigma_B}\right) \tag{3.24}$$

where L_B is the width of the membrane (electrode to electrode), and σ_B is the conductivity of the membrane (proton conductivity). The whole polarization equation was then brought together by substituting all parts of the polarization model. As mentioned earlier, to simplify the polarization of the cell, the two reactions that occur on the cathode (ORR and HER), depending on the current density of the cell, were modeled as if they occurred independently. This is an accurate assumption

at very lower current densities and at very high current densities as one reaction will be very dominant over the other. This is not the case however during the transition point ($i_r \rightarrow i_{r,L}$) as they both had roughly similar kinetics. For this model, two different equations were used to describe the polarization of the cell. One with the ORR on the cathode and OER on the anode for lower current densities and one with the HER on the cathode and OER on the anode for current densities that have surpassed the limiting current density on the cathode. These two polarization sections are described as "OxyGen Operations" and "PEM-WE Operations" respectively.

Equation 3.4 can be rewritten to give a direct relationship for the potential on the electrodes given a current density:

$$\Phi_a = \eta_{r,a} + \Phi_{r,0} \tag{3.25}$$

Using equation 3.22 describing the overpotential on the anode, the positive potential can be found:

$$\Phi_+ = \Phi_{OER,0} + \left(\frac{RT}{\alpha_{OER}F}\right)\sinh^{-1}\left[\frac{1}{2}\left(\frac{i_{OER,+}}{i_{OER,0}}\right)\right] \tag{3.26}$$

Where $i_{OER,+} = i^+ = i$ as the OER was the only reaction to occur on the positive electrode. Combining equations 3.23, 3.24, and 3.26 provided a polarization function based on the current density and the potential at the negative electrode:

$$V = \Phi_{OER,0} + \left(\frac{RT}{\alpha_{OER}F}\right)\sinh^{-1}\left[\frac{1}{2}\left(\frac{i_{OER,+}}{i_{OER,0}}\right)\right] + i_B\left(\frac{L_B}{\sigma_B}\right) - \Phi_- \tag{3.27}$$

The potential on the negative electrode is a function of the current density supplied to the cathode containing two simultaneous reactions. The overall negative electrode current density is the sum

of the current density supplied to the ORR and HER as shown in equation 3.3, the total

overpotential must also be the summation of the overpotentials created from the two reactions:

$$\eta_- = \eta_{ORR,-} + \eta_{HER,-} \tag{3.28}$$

The overpotentials for the respective reactions can be found from equation 3.21. Like the OER,

the limiting current density pertaining to the HER is large (i << $i_{HER,L}$) and can take a similar form

as equation 3.22:

$$\eta_{ORR,-} = \left(\frac{RT}{\alpha_{ORR}F}\right)\sinh^{-1}\left[\frac{1}{2}\left(\frac{i_{ORR,-}/i_{ORR,0}}{1 - i_{ORR,-}/i_{ORR,L}}\right)\right] \tag{3.29}$$

$$\eta_{HER,-} = \left(\frac{RT}{\alpha_{HER}F}\right)\sinh^{-1}\left[\frac{1}{2}\left(\frac{i_{HER,-}}{i_{HER,0}}\right)\right] \tag{3.30}$$

These equations can be rearranged to find the current densities for each reaction given an

overpotential. Combining these equations with equation 3.4 showing the overpotential in terms of

the potential at the negative electrode, the current densities can be found by:

$$i_{ORR,-} = \frac{2\sinh\left(\frac{\alpha_{ORR}F(\Phi_- - \Phi_{ORR,o})}{RT}\right)}{\frac{1}{i_{ORR,o}} + \left(\frac{1}{i_{ORR,L}}\right)2\sinh\left(\frac{RT}{\alpha_{ORR}F}\right)} \tag{3.31}$$

$$i_{HER,-} = \left(i_{HER,o}\right)2\sinh\left(\frac{a_{HER,-}F(\Phi_- - \Phi_{HER,0})}{RT}\right) \tag{3.32}$$

The total current density at the negative electrode can then be found by equation 3.3 by adding equations 3.31 and 3.32.

$$i_- = i = \frac{2\sinh\left(\frac{\alpha_{ORR}F(\Phi_- - \Phi_{ORR,o})}{RT}\right)}{\frac{1}{i_{ORR,o}} + \left(\frac{1}{i_{ORR,L}}\right)2\sinh\left(\frac{RT}{\alpha_{ORR}F}\right)} + (i_{HER,o})2\sinh\left(\frac{\alpha_{HER,-}F(\Phi_- - \Phi_{HER,0})}{RT}\right) \tag{3.33}$$

This equation was used to find the negative electrode potential for any current density supplied to the cathode. The need to operate the reactions separately during the two current density operating parameters ($i_- < i_L$ and $i_- > i_L$) was now bypassed and one continuous equation using the polarization relationship from equation 3.27 is used.

OxyGen Operations
($i < i_L$)

$$V = \frac{RT}{4F}\ln\left(\frac{p_-}{p_{O_2,-}}\right)\left(\frac{p_{O_2,+}}{p_+}\right) + \left(\frac{RT}{\alpha_+ F}\right)\sinh^{-1}\left[\frac{1}{2}\left(\frac{i_+}{i_{+,0}}\right)\right] -$$
$$\left(\frac{RT}{\alpha_{ORR,-}F}\right)\sinh^{-1}\left[\frac{1}{2}\left(\frac{i_{ORR,-}/i_{ORR,-,0}}{1 - i_{ORR,-}/i_{ORR,-,0}}\right)\right] + i_B\left(\frac{L_B}{\sigma_B}\right) \tag{3.34}$$

PEM-WE Operations
($i > i_L$)

$$V = 1.229\,V - 8.46x10^{-4}(T - 298K) + \left(\frac{RT}{4F}\right)\ln\frac{a_{H_2}^2\left(p_{O_2}/p_+\right)^{\frac{1}{2}}}{a_{H_2O}} +$$
$$\left(\frac{RT}{\alpha_+ F}\right)\sinh^{-1}\left[\frac{1}{2}\left(\frac{i_+}{i_{+,0}}\right)\right] - \left(\frac{RT}{\alpha_{HER,-}F}\right)\sinh^{-1}\left[\frac{1}{2}\left(\frac{i_{HER,-}}{i_{HER,-,0}}\right)\right] + i_B\left(\frac{L_B}{\sigma_B}\right) \tag{3.35}$$

For both equations, it was now assumed that all current densities were equal for the electrodes and the membrane ($i_- = i_+ = i_B = i$). Using the same reasons for the OER neglecting the limiting current density term in equation 3.22, the same can be said for the HER when the operation condition

subjected to the cell is $i_{HER,-} << i_{HER,L}$ and can be simplified. Although the overpotential terms in both equations are different, the primary driving force resulting in the abrupt change in polarization was the equilibrium potential going from zero to that of a normal PEM electrolyzer. If developed, the OxyGen model will never operate within PEM-WE operations, however the parameters of such operations are modeled for theoretical purposes.

3.3 Mass Balance

In order to complete the terms provided in the polarization equation, a mass balance of all species will be conducted to determine activities at specific current densities. Portrayed in figure 3.3 is the CSTR (continuous stirred tank reactor) model of the OxyGen cell where n_α is the molar flow rates of all species in the system.

$$O_2$$
$$N_2$$
$$\downarrow$$

$$H_2O$$
$$O_2$$
$$\uparrow$$

$4H^+ + O2 + 4e^- \rightleftarrows 2H_2O$

H^+

$2H_2O \rightleftarrows 4H^+ + O2 + 4e^-$

Cathode

$\leftarrow$

Anode

$2H^+ + 2e^- \rightleftarrows 2H_2$

$$\downarrow$$

$$\uparrow$$

$$O_2 \qquad N_2$$
$$H_2O \qquad H_2$$

$$H_2O$$
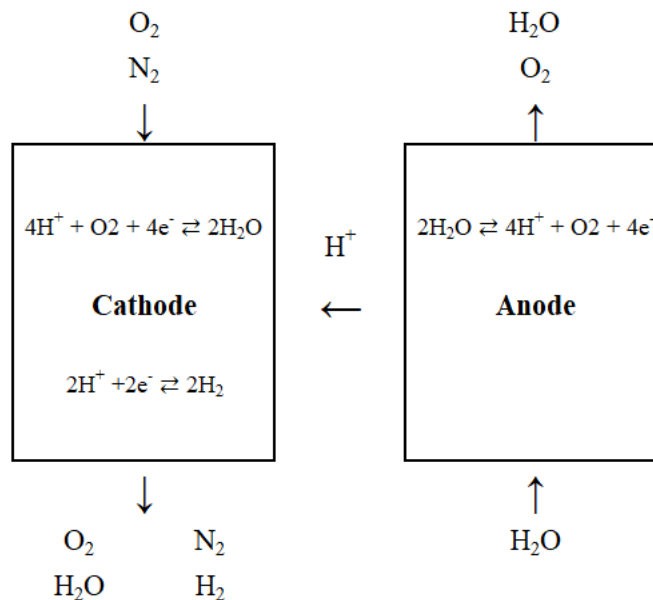
Figure 3.3. CSTR mass balance model of an OxyGen cell

3.3.1 Water (anode)

Water in the anode was used as a typical PEM-WE raw material and will only act in the OER. The amount of water that was reacted was dependent on the current density in the anode, i_-, but as mentioned before, the assumption of constant current density across the cell still holds. The actual current in the cell was used to find the number of electrons transferred by multiplying the current density by the area of the membrane to find the current, I. The mass balance of the water in the anode was then explained by:

$$n_{+,H_2O,out} = n_{+,H_2O,in} - \frac{I}{|v_{+,e-,H_2O}|F}$$
(3.36)

where $v_{+,e-,O_2}$ is the number of electrons representing one mole of oxygen in the OER equation on the anode. As mentioned before, enough water was supplied to the cell such that the amount of water present would not affect the diffusion limitations of the anode at operating voltages and current densities. For all trials, the inlet of the water was a constant rate.

3.3.2 Oxygen (anode)

As with water in the anode, the mass balance of oxygen in the positive electrode will behave as a typical PEM-WE. The oxygen generation from the OER is dependent on the total current, I, and is explained by the equation:

$$n_{+,O_2,out} = \frac{I}{|v_{+,e-,O_2}|F}$$
(3.37)

As mentioned above, the oxygen that is produced on the anode may lead to difficulties of the water binding to the active sites on the catalyst because of bubbling and interference, but this is neglected and the limiting current density is much larger than any operating current density (i << i$_{+,L}$).

3.3.3 Proton Transfer Balance (Membrane)

Again, the number of protons transferred from the anode to the cathode will behave as a PEM-WE model with respect to the anode. The rate the OER will generate protons for transfer across the membrane is dependent on the current of the electrons explained by the formula:

$$n_{H^+,trans} = \frac{I}{|\nu_{+,e-,H^+}|F}$$

(3.38)

where $n_{H^+,trans}$ is the molar flow rate of the protons that are transferred across the membrane.

3.3.4 Oxygen (cathode)

The mass balance of oxygen in the cathode will behave as a typical proton exchange membrane fuel cell (PEM-FC) as it was used as a reactant in the ORR on the negative electrode. The flow rate of the species will be dependent on the current of the electrons transferred from the anode, as it decreases with an increased current density. This is only true up until the current density reaches the limiting current density, where the ORR will lose favorability to the HER and continue to operate at the same rate for any increased current density. As part of the study, the flow rate of the inlet air will vary to observe its impact, and this rate of entry will also influence the total flow rate of air and theoretically the limiting current density. The mass balance is described as:

$$n_{-,O_2} = n_{-,O_2,o} - \frac{I}{|\nu_{-,e-,O_2}|F} \qquad (i < i_{-,L})$$

$$n_{-,O_2 t} = n_{-,O_2,o} - \frac{I_{-,L}}{|\nu_{-,e-,O_2}|F} \qquad (i > i_{-,L})$$

(3.39)

and can be rewritten in terms of the molar flow rate of air, knowing the concentration of oxygen

in air as 21%:

$$n_{-,O_2} = (n_{-,air} * 0.21) - \frac{I_{ORR,-}}{|\nu_{-,e-,O_2}|F} \qquad (i < i_{-,L})$$

$$n_{-,O_2} = (n_{-,air} * 0.21) - \frac{I_{ORR,-,L}}{|\nu_{-,e-,O_2}|F} \qquad (i > i_{-,L})$$

(3.40)

3.3.5 Water (cathode)

As with the oxygen balance on the cathode, the water balance on the negative electrode will follow

a similar behavior to a PEM-FC. The water is generated from the ORR and is dependent on the

current transferred from the anode. The same phenomenon occurs once the current density

surpasses the limiting current density of the cathode and the flow rate will remain constant for any

increase in i as the ORR will be reacting at the same rate due to the HER feasibility. The equation

to describe the mass balance is:

$$n_{-,H_2O} = \frac{I}{|\nu_{-,e-,H_2O}|F} \qquad (i < i_{-,L})$$

$$n_{-,H_2O} = \frac{I_{-,L}}{|\nu_{-,e-,H_2O}|F} \qquad (i > i_{-,L})$$

(3.41)

It should be mentioned that the recommended prototype of the OxyGen model would recycle this

generated water back to the anode to be electrolyzed. This creates a closed loop regarding the

entire mass balance of water, meaning the only raw material needed for the system would be air. Depending on the operating temperature of the system, water may be lost due to evaporation and may need to be replenished if too much water has been lost.

3.3.6 Hydrogen (cathode)

Hydrogen gas is only produced if i surpasses $i_{-,L}$, where the HER will occur and is considered an undesirable product. The production of the gas will follow behaviors related to PEM-WE operations in the negative electrode. The current of electrons that lead to the production of hydrogen will be denoted as $i_{-,HER}$ as per equation 3.3. The mass balance is seen as:

$$n_{-,H_2,out} = \frac{I_{-,HER}}{|\nu_{-,e-,H_2}|F}$$

(3.42)

3.3.7 Nitrogen (cathode)

Nitrogen is an inert gas in the case of the OxyGen model because it does not react in either reaction taking place on the negative electrode. It is only dependent on the inlet flow of air into the cathode. It is important to keep this species in mind to establish the activities of other species affecting the limiting current density and diffusive properties. It was assumed that nitrogen makes 79% of air.

Molar Composition of Oxygen (Cathode)

$$x_{-,O2} = \frac{n_{-,O2}}{n_{-,O2} + n_{-,N2} + n_{-,H2O} + n_{-,H2}}$$

(3.43)

ORR Limiting Current Density (Cathode)

As mentioned before, the gas inside the cathode chambers was treated as ideal, meaning the activity of oxygen will be its molar composition. Substitution of equation 3.43 into the definition of the limiting current density shows the following:

$$(i_- < i_{-,L})$$

$$i_{ORR,L} = 4FPc_i^o \left(n_{-,O_2,o} - \frac{I}{|v_{-,e-,O_2}|F} \right) * \left(\frac{1}{n_{-,N2} + \left(n_{-,O_2,o} - \frac{I}{|v_{-,e-,O_2}|F} \right) + \frac{I}{|v_{-,e-,H_2O}|F}} \right) \tag{3.44}$$

The hydrogen molar flow term is taken out of the equation because once the current density supply for the ORR surpasses its limiting current density, the current, I, will remain constant for any increase in potential.

4. Experimental Methodology

4.1 Electrolyzer Materials and Assembly

To conduct the experimentation required for this project, a list of components had to be purchased, with the goal of customizing the current PEM electrolyzer cell to our needs. As previously mentioned, a 50 cm² cell structure along with the corresponding graphite plates already existed in the lab. The pre-existing bipolar plates can be seen below in figure 4.1.
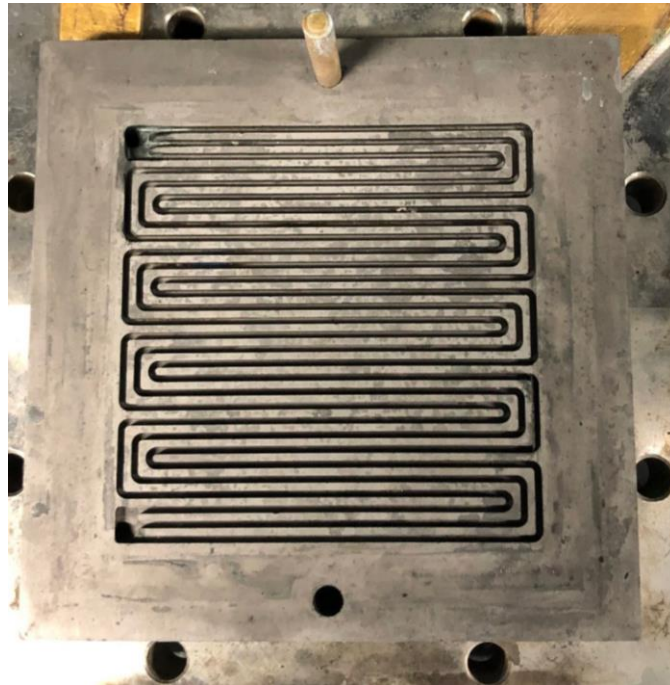
Figure 4.1. Serpentine Bipolar Plates with a 50 cm² active site

This meant an entire MEA, specific to our research and goals, had to be purchased, along with Ultem spacers to distribute compression properly and silicon gaskets to seal the system. The team acquired two 10 by 10 cm titanium screen meshes that were 0.01 inches thick to act as one version of our GDL and two 10 by 10 cm sheets of carbon Toray paper to act as an alternate GDL material. A 50 cm² CCM was purchased, composed of Nafion 115 and coated with 3 mg/cm² of Iridium

Ruthenium Oxide on the anode side and 3 mg/cm^2 of Platinum black on the cathode side. These three components put together were what was used for the MEA and will be the main "engine" for electrolysis. Outside of these MEA components were the Ultem spacers used to distribute compression in an inequivalent manner. Compressing the carbon paper, titanium mesh, and CCM equivalently in the cell can cause the titanium mesh to indent and even puncture the CCM since it has a high compressive resistance. Equal compression can also introduce conductivity problems and the closure of pores in the CCM and carbon paper which can and will hinder the transfer of protons. Ideally, the carbon paper will experience around 20 percent compression with the CCM and titanium mesh not compressing at all. A diagram of the internals, including the spacers, silicon gaskets and MEA can be seen below in figure 4.5. To build the cell, one of the titanium mesh sheets and carbon toray paper sheets were cut down to the size of the CCM's active area of 50 cm^2. The cut versions of each can be seen below in figures 4.2 & 4.3.
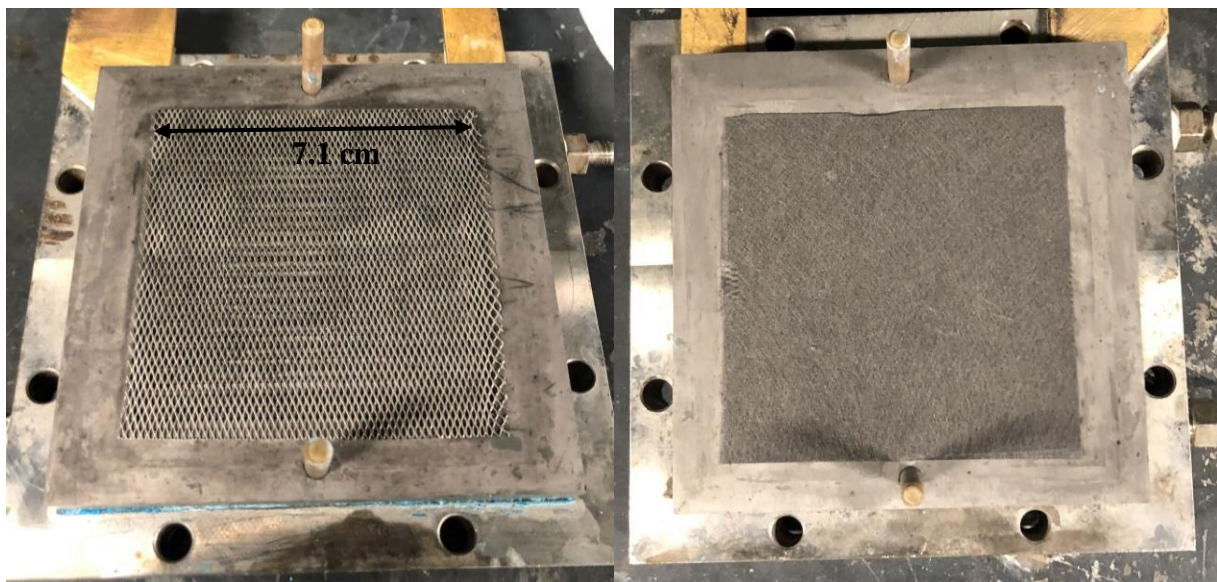
Figures 4.2 & 4.3. Non-platinized Titanium Mesh (left) & Carbon Toray Paper (right) on Bipolar plates

Once done, the titanium mesh was placed on the anode side of the MEA and carbon paper GDL

was placed on the cathode side. All three were lightly painted with a Nafion wetting solution

already present in the lab to ensure that proper conductivity between the materials was achieved.

Next, two separate Ultem rings were cut for each side of the MEA (4 total). These can be seen

below in figure 4.4.
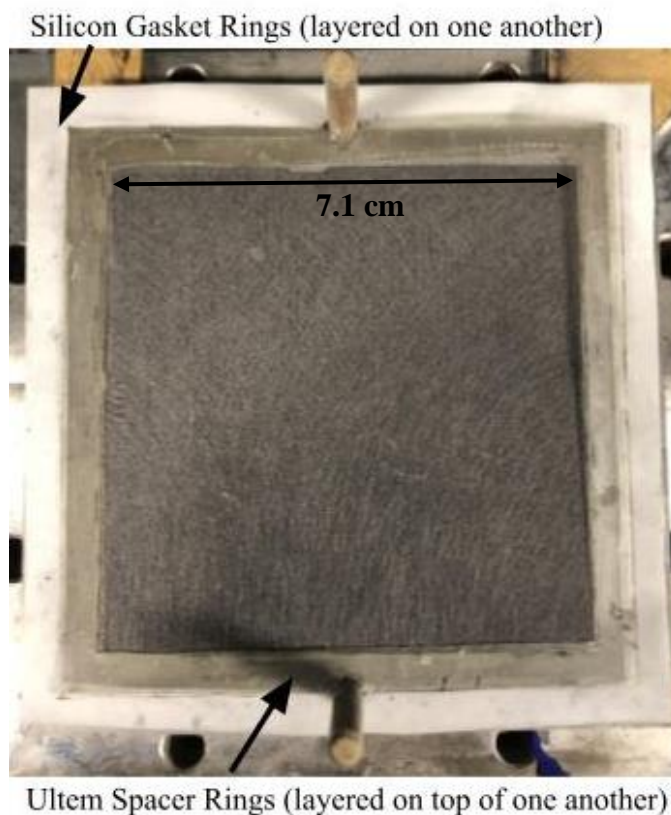
Figure 4.4. Internal view of the layered material within the cell

by the light blue sections on the outside of GDL's. For the anode side of the cell, one 0.005 inch

thick Ultem ring (10x10 cm, 1.47 cm width) and one 0.003 inch thick Ultem ring (8.75x8.75 cm,

0.835 cm width) spacers were cut. Similarly, for the cathode side of the cell, two 0.003 inch thick

Ultem ring spacers were cut to the same sizes as the ones on the anode side of the cell. These

spacers were layered according to the diagram below on the MEA. Two square 10 by 10 cm rings (0.635 cm in width) of silicon were cut and placed on the outside of the spacers on each side (seen in the figure below by the white sections touching the bipolar plates) and then each graphite bipolar plate was placed on the sides, making sure that the active areas of the membrane were in line with the serpentine channels of the plates. Finally, the outer shell plates were connected on either side of the bipolar plates and bolted together. It is important to note that the bolts were tightened in a cross pattern fashion using a torque wrench to achieve the same degree of compression throughout the entire cell. It was determined that 10 N*m of torque was adequate for the system because it both prevented water leakage from occurring and caused little to no noticeable problems with the MEA components.
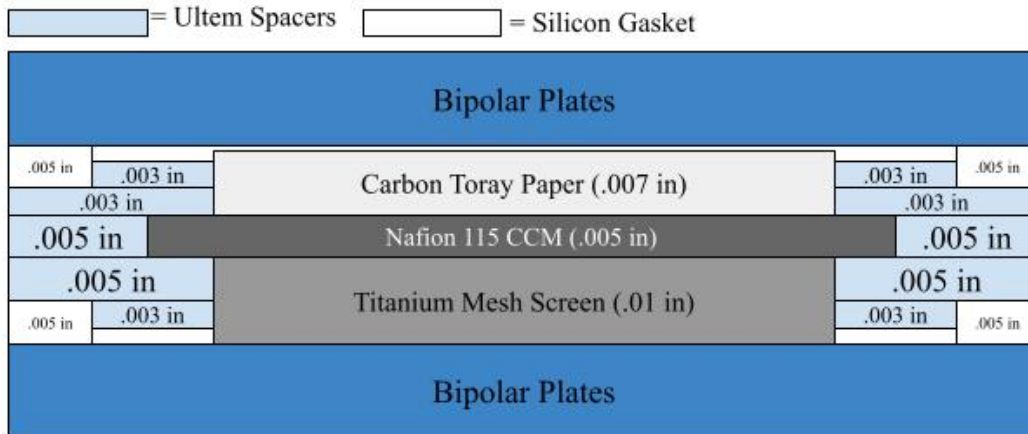
Figure 4.5. Cell Internals Diagram of Experimental Electrolyzer

The completely assembled electrolyzer cell can be seen below in figure 4.6.

Figure 4.6. Completely assembled cell structure with all internal MEA components enclosed within the graphite bipolar plates in the middle

4.2 System Setup

To operate the system described above, a reasonable amount of equipment, tubing, and electrical components are required for it to function correctly. A general schematic of the system setup can be seen below in figure 4.7.
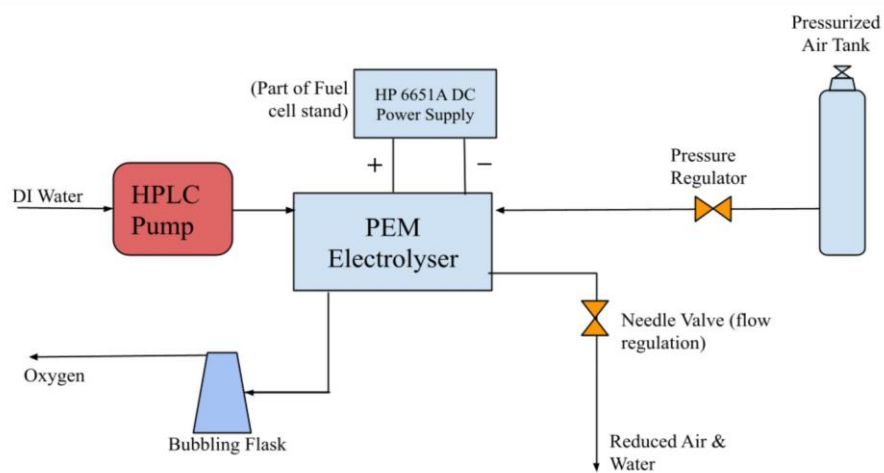
Figure 4.7. Schematic of the experimental setup required for the experiment

Each side of the electrolyzer cell has an input and output tube with different compounds flowing through them depending on their function. On the inlet of the anode side (seen on the left side of figure 4.7), there was distilled water flowing into the system through 1 cm O.D tubing. An HPLC pump connects a storage of distilled water to the cell and allows us to run different flow rates of water into the system depending on the experimental variation being performed. On the outlet of the anode side is the produced humidified oxygen or product outlet. A displacement flask will be connected to this tubing so that it can be determined for one, if oxygen is being produced, and two, to collect the gas by displacing the water inside of it so that volumetric measurements of the gas can be performed. On the cathode side of the cell, there is an inlet for air. This inlet is connected to a pressurized Airgas 30-liter cylinder of Grade Ultra Zero air with the flow rate regulated by a pressure regulator on top of the cylinder. The outlet for this side will contain both gas and liquid and is essentially a waste stream for this experiment but would feed back into a recycle stream in a final product. It will contain any excess air molecules (largely nitrogen) and water that has formed from the hydronium ions and oxygen molecules. For the experimental variation where no air flow is occurring (normal PEM electrolysis), an inverted graduated cylinder was placed at the end of this waste stream so that the hydrogen produced could also be measured in order to determine if the expected stoichiometric ratio of hydrogen and oxygen were being produced. To power the cell, the Hewlett Packard 6651A System DC Power Supply was used. Initially, this power supply was wired in junction to the Fuel Cell test stand which allowed for data to be relayed to the connected computer program. This connection also allowed for the applied current and voltage to be manipulated systematically. Unfortunately, issues arose during testing which resulted in the Fuel Cell test system to be circumvented, meaning a direct connection between the anode

and cathode of the cell to the HP power supply was used. This allowed for more accurate readings of the voltage and current density being applied to the cell since the resistance from the Fuel Cell testing system was removed. In addition to the direct readings of voltage and current from the HP power supply (which were manipulated by simply adjusting a dial), a multimeter located in Goddard Hall 017 was connected directly to the cell electrodes to produce the most accurate data possible of voltage, current density, and even resistance across the cell. Figure 4.8 below, shows what one of our experimental setup variations looked like early on when the cell was being tested.
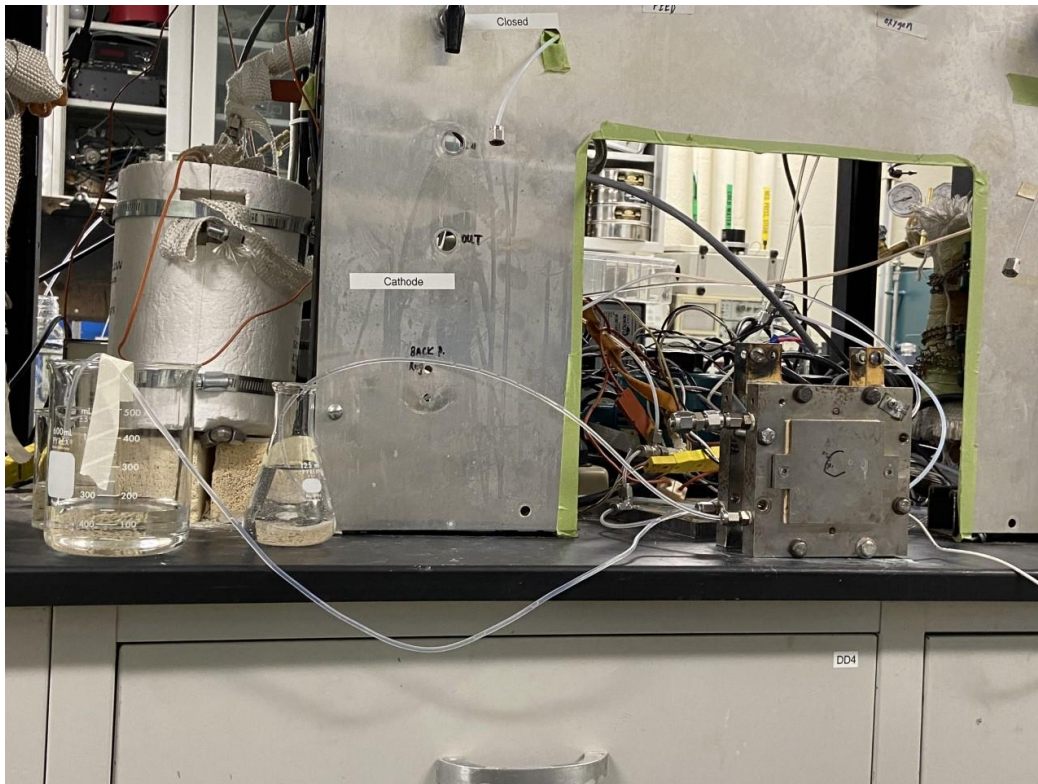
Figure 4.8. Early stage setup of experimentation (normal electrolysis with no gas collection)

4.3 Experimental Procedure

After the apparatus had been successfully assembled, with the fuel cell attached and able to send varying voltages as well as tubing attached to the anode and cathode for the provision of water and

air streams into the system, experimental trials were able to begin in order to collect data. The primary initial focus of data collection was to determine the effect of flow rate variance for the air stream, as well as the effect of providing varying voltages to the system. Before including the air stream though, basic electrolysis would be tested by just including the water stream as an input rather than both the water and air streams. These tests were first performed on a smaller electrolyzer with a 5 cm^2 MEA before moving on to tests on the full sized 50 cm^2 MEA in order to reduce risk of damage. The goal of running the electrolyzer with just the water stream was to both confirm oxygen and hydrogen production as well as to ensure expected current ranges were being produced before adding in the air stream. It was important to start initial experimentation with low flow rates and voltages to prevent damages to the assembly when the upper limit of how much flow or voltage the system can operate under is not clearly defined. Water flow rates were initially implemented at amounts of less than one milliliter per minute (0.75 milliliters per minute). Air flow rates, when they would eventually be implemented, would range from around 0.2 to 1.0 Liter. There was less concern for higher air flow rates than there was with water as there was no risk of flooding the system with certain air flow rates like there was for water, so higher flow rates for air can be more safely used. As for voltage, each trial would begin at voltages of less than 1.0 V, before gradually increasing the voltage until around 1.8 V was reached. Voltages higher than this point would generally not be tested in order to prevent damage to the cell. Once testing with both the air and water streams included would begin, the primary two factors that would be varied would be the air stream flow rate and the voltage. At a specific air stream flow rate, the same range of voltages would be tested before again changing the air flow rate and repeating the same process.

The current density in each trial was closely monitored as well as any production of hydrogen or oxygen.

After initial experimentation, adjustments could be made to the system in order to improve performance and increase the overall current and gas production. The primary method for improving performance was to adjust the overall compression on the cell. If the cell were tightened too excessively, the titanium mesh would compress too far into the MEA and create imprints, hindering the cell's ability to create adequate currents. On the other hand, if the cell is too loose, there will not be enough contact for proper electrolysis to occur. The use of the spacers included in the cell's design would allow for these compression adjustments to determine the optimal level of compression for proper electrolysis to occur. Other conditions could also be varied as much as time permitted to improve cell performance. The first of which being the temperature that the system runs under. All initial testing was done under conditions at room temperature with relatively no variance. As shown in Figure 2.5, as temperature increases, cell performance increases. Working with liquid water in the anode adds limitations as if it is heated too much, water vapor will block active sites on the $IrRuO_2$ catalyst and prevent oxygen from exiting the anode. The optimal temperature found is 80℃ before performance is altered [22]. Temperature values ranging from 40 to 60 to 80 degrees Celsius were able to be tested to get a proper range of results. While these temperature variances were not expected to have a significant effect on the current output and gas production, optimizing the temperature could prove to help optimize the whole process. One other factor worth mentioning that could be varied for data collection would be the pressure of the system. Testing different pressure ranges could be done by using a back pressure regulator to control the pressure of the air stream entering and leaving the system. Assuming initial

conditions of approximately 1 atm, the pressure of the air stream could be increased to values of 1.5 to 2 atm to potentially as high as 3 atm's to determine the overall effect this has on oxygen and hydrogen production. While the time frame allotted did not allow for pressure variance tests to be performed, future experimentation following this research could perform these attempts to further optimize the process.

5. Results & Discussion

5.1 Theoretical Polarization

Using the stitched equations from equations 3.34 and 3.35, a predicted polarization of the OxyGen electrochemical model was plotted as cell potential vs current density seen below in figure 5.1. The parameters for each reaction can be found in appendix A.
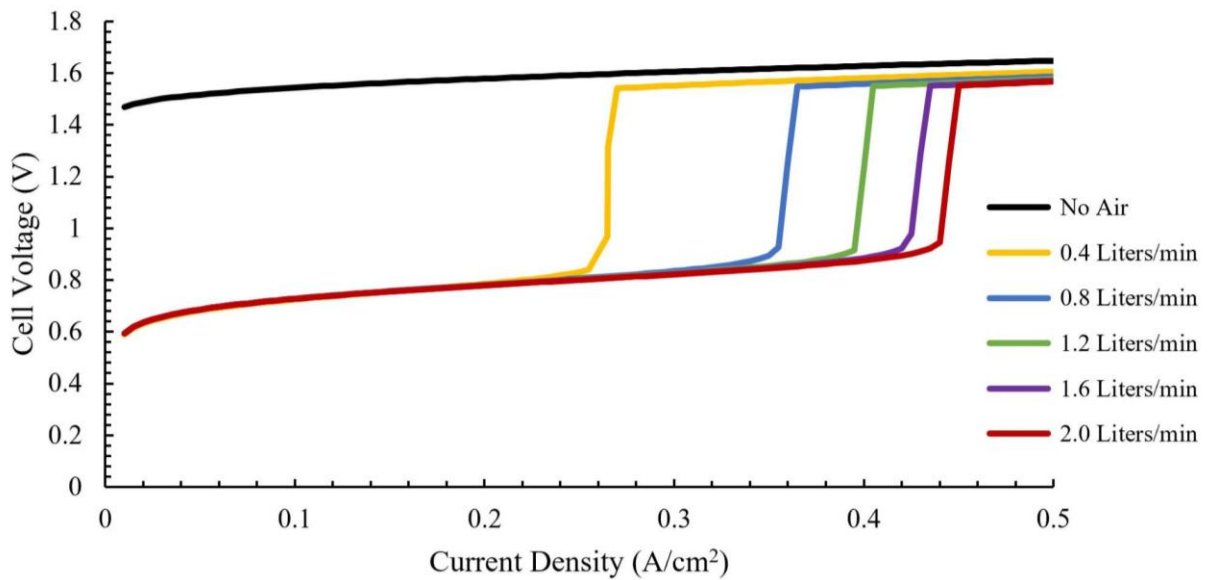
Figure 5.1. Polarization of OxyGen model given varying ambient air volumetric flow rates (0-2 /min)

Using the same parameters describing the reactions in the polarization plot, the individual potentials on the electrodes were obtained from equations 3.26 and 3.33. As mentioned before, instead of an instantaneous transition of equations, only one equation is used to describe the cathode potential using the relationship of i_- ($i_- = i_{ORR,-} + i_{HER,-}$). The resulting graph was used for a single flow rate to show the effects the current density has on the potentials. The only prominent effect of the air flow into the cathode would be the asymptotic behavior of the cathode potential before HER feasibility becomes relevant based on the limiting current density of the electrode.

A reaction is deemed feasible if $(v_{re\text{-}})\eta_{r,a} > 0$ where the overpotential is found by: $\eta_{r,a} \equiv \Phi_a - \Phi_{r,0}$.

The following reactions are:

$$
\begin{aligned}
&\text{OER: } 2H_2O \rightleftharpoons O_2 + 4H^+ + 4e^- \\
&\text{ORR: } O_2 + 4H^+ + 4e^- \rightleftharpoons 2H_2O \\
&\text{HER: } 2H^+ + 2e^- \rightleftharpoons H_2 \\
&\text{HOR: } H_2 \rightleftharpoons 2H^+ + 2e^-
\end{aligned}
$$
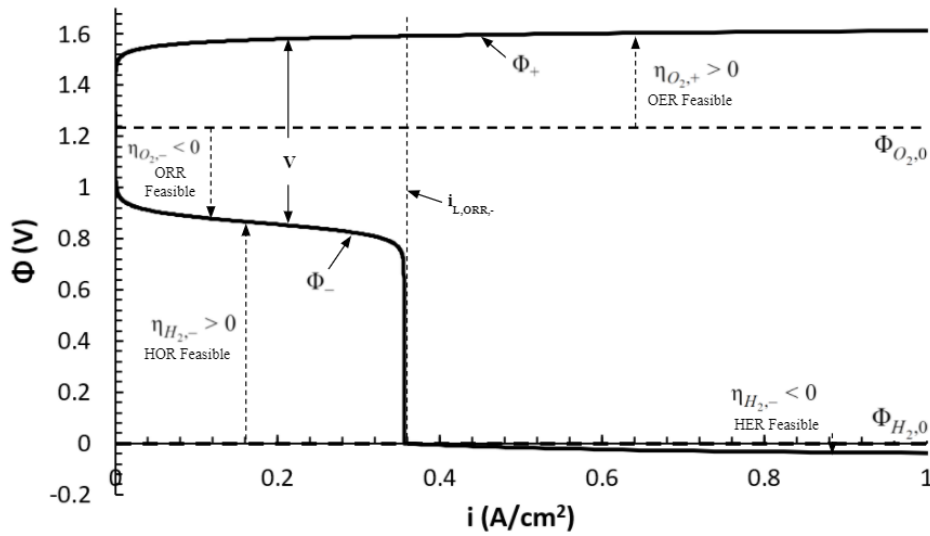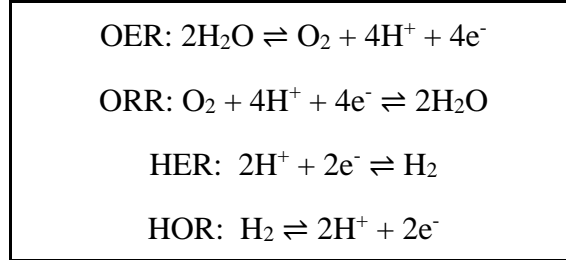
Figure 5.2. Electrode potential vs current density indicating reaction feasibility with an ambient air intake of 0.8 L/min. External voltage needed to be supplied to the cell is explained by the difference in electrode potentials (Φ_+ - Φ_-). The surpassed limiting current density is outlined in the polarization as the vertical asymptote exhibited on the negative electrode potential polarization. $v_{ORRe\text{-}}$ and $v_{HERe\text{-}}$ are negative and the respective reactions will be feasible once their overpotentials are negative. $v_{OERe\text{-}}$ and $v_{HORe\text{-}}$ are both positive and will be feasible with positive overpotentials.

5.2 Literature Comparison

Due to lack of funds, PEM operation inexperience, and other sources of error, our team was unable to produce sufficient results to compare to our produced model of the polarization of the OxyGen system. To see how well the model held up to experimental data, the model was set to predict the polarization of an oxygen pump operating at 80°C and 1 atm pressure in a $50cm^2$ cell being supplied ambient air at 0-2 L/min (0, 0.4, 0.8, 1.2, 1.6, and 2 L/min) in order to see how well it compared to experimental data presented by CSIRO Energy Technology [16]. Below are the polarization plots of the six different air flow rates of the oxygen pump comparing the model and the experimental data:

a) No Cathodic Air Flow b) 0.4 Liters/min Air Flow

c) 0.8 Liters/min Air Flow d) 1.2 Liters/min Air Flow

e) 1.6 Liters/min Air Flow f) 2.0 Liters/min Air Flow
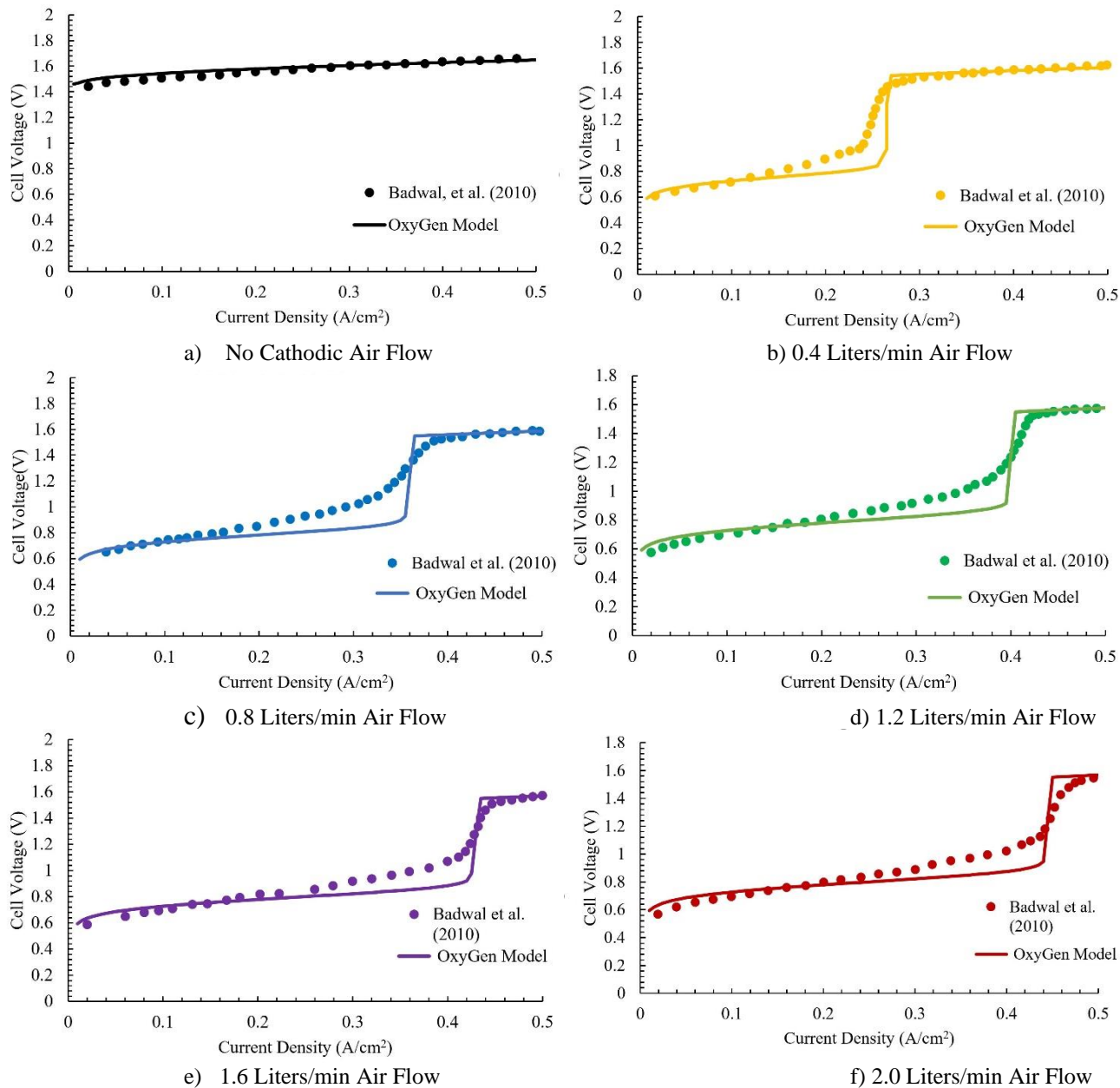
Figure 5.3. Modeling polarization comparison with 2010 literature experimentation

As seen in Figure 5.3, the model predicts the polarization of the experimental collected data exceptionally well at low current densities and high current densities for all flows tested. The coefficient of determination was found for all plots and found the average was 82.5% ($R^2 = 0.825$). Although the correlation between potentials given a current density between the model and the

experimental results are not up to statistical standards, the biggest discrepancy seen in the plots are at the transition points. The transition points for each flow rate are predicted quite accurately ($\pm$ 0.005 A/cm^2) based on the limiting current density of the negative electrode; the polarization in this section is not predicted well. This outcome can be described by the assumptions made in section 3.1 about reactions occurring independently in order to simplify the equations to make a relationship for the polarization. As predicted, the model produces a sharp increase at the transition point when the reactions switch over while the experimental data show a more gradual slope from oxygen pump operations to PEM-WE. Although the model is not completely accurate for all current densities, for the purpose of the OxyGen system, it will be operating with lower current densities while the ORR is still the favorable reaction.

5.3 Surpassing Limiting Current Density

The limiting current density in electrochemical systems is the maximum the current density can be to still achieve the preferred reaction on an electrode without additional reactions to occur or extraneous ions produced. Stoichiometric, species activity, and permeance describe how the limiting current density is determined on an electrode for a specific reaction as seen in equation 3.18. Limiting current density is caused by a stoichiometric limitation from the lack of the reacting species, oxygen, on the catalyst to react with the protons transferring across the membrane. Although there may still be plenty of oxygen still in the electrode chamber, the diffusive flux of the species, described as the permeance in the limiting current density equation, is counteracted by the flux of the species through the outlet of the chamber. Overall, it is the stoichiometric limitations

that lead to the limiting current density, the diffusing properties lead to a specific limiting current density on the electrode.

Limiting current density will not stay constant throughout the cell's polarization operations. The species activity is dependent on the mass balance of oxygen in the negative electrode. Described in equation 3.39, any increase in the cell current density will deplete the composition of oxygen gas in the electrode, thereby decreasing the limiting current density for the ORR as more voltage is applied to the system. As seen in Figure 5.4, the ambient air volumetric flow rate affects the limiting current density as it is surpassed by the current density of the cathode in a positive relationship with a horizontal asymptote as $v_o \rightarrow \infty$. Fick's Law describes this phenomena because as more oxygen is introduced into the cathode at higher flow rates for any current density, the disappearance of the species will be the same but the bulk concentration is greater through the higher rate of oxygen replacement [27]. Comparing the below graph to Figure 5.1, as the air flow rate increases, the limiting current density continually increases but at slower rates for higher v_o values, explaining the tighter transition points across the evenly distributed flow rates at higher rates.
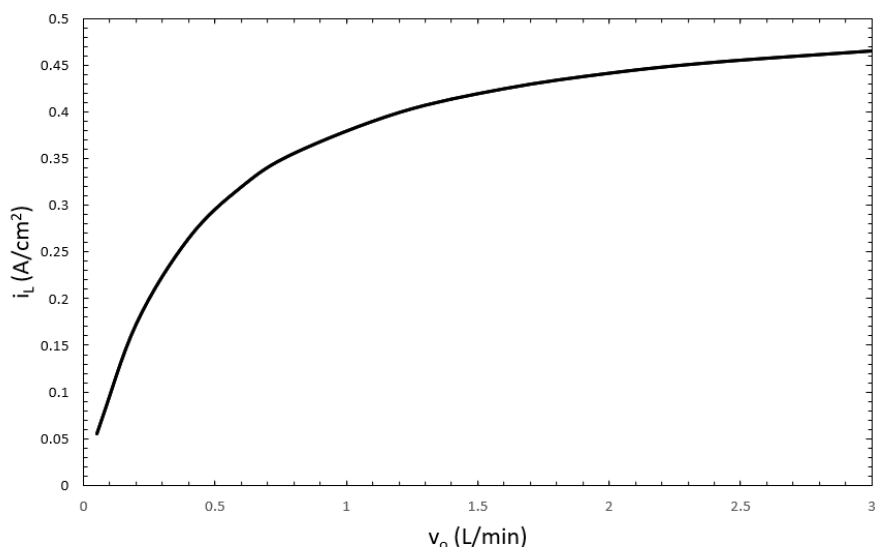
Figure 5.4. Limiting current density as it is surpassed by current density dependence on volumetric air flow

Using the parameters of the ORR in the negative electrode given a very high flow rate of air into the system (1×10^9 L/min air), the maximum limiting current density was found to be 0.52 A/cm^2. This is an unrealistic flow rate for actual operations as the expense, hassle, and cell damage would outweigh the benefits of the system, providing an exceptional current density for a low voltage.

5.4 Experimental Limitations

As mentioned previously, the experimentation portion of this project did not produce data comparable to the Badwal et. al 2010 report. After much analysis and ultimate failure to self-diagnose the problem, the expertise of local electrolyzer expert, Patrick Emerick, was sought out for further knowledge. Ultimately, there were a large number of "smaller" problems that Patrick was able to identify for the team that when added together, likely were the main causes of our cells' inefficiency [28]. The list below is a breakdown of issues with the experimental unit:

- No Microporous Layer - The absence of a microporous layer (MPL) is the first of the possible problems with our cell. An MPL is used as a layer between the GDL and the catalyzed membrane to prevent the loss of catalyst to the GDL and to minimize the contact resistance between the two layers. This introduced the possibility that some of the catalyst was lost to either GDL, ultimately creating inefficient electrolysis [28]. The MPL is also useful in that it provides effective water transport near the CCM increasing the number of active oxygen sites for better electrolysis.

- Corroded electrodes - To the untrained eye, this was not an obvious problem. The electrodes on the current cell were originally gold plated to help prevent corrosion. However, most of the gold plating was gone by this point meaning that the electrodes had likely been oxidized, therefore increasing their resistance to current flow [28].

- Graphite Anode Bipolar Plate - Another potential issue with the cell was the use of a graphite bipolar plate on the anode side of the cell. As previously discussed in chapter 2, a titanium bipolar plate is useful for the anodic side of the cell to prevent oxidation of the graphite. Given that it is unknown how long this plate has been used in the cell, it is very likely that significant oxidation had occurred but due to lack of funding, a more effective titanium plate was not acquired [28]. Figure 5.5 illustrates the possible oxidation that had occurred as well as the likely deterioration that will be further explained below.

Figure 5.5. Deteriorated and oxidized graphite bipolar plate

- Deterioration from vicious reaction - Patrick Emerick recalled, once seeing the cell in person, that it was used in a very aggressive reaction that destroyed a while back [28]. Whilst the team was unable to locate the project to specifically determine what reaction had occurred, it is likely that this introduced macroscale deterioration of the bipolar plates, invisible to the naked eye.

- Bipolar Plates too small (outside of active area) - It was also determined that the surface surrounding the active area of the bipolar plates was too small to effectively have Ultem spacers used [28]. As previously mentioned, this space was approximately 1.55 cm wide which made the goal of compressing specific components more than others for effective conductivity hard to achieve.

- Nafion Dried Out - Another possible problem with the experimental portion of the project was the Nafion drying up. Since this was a long term project (experimentation over the course of 5 months), it's very likely that the CCM (Nafion) dried out, introducing the

possibility of small scale cracks in the membrane [28]. These would interfere with proton transfer across the Nafion and allow for water leakage through it. A picture of the dried out membrane can be seen below in figure 5.6.
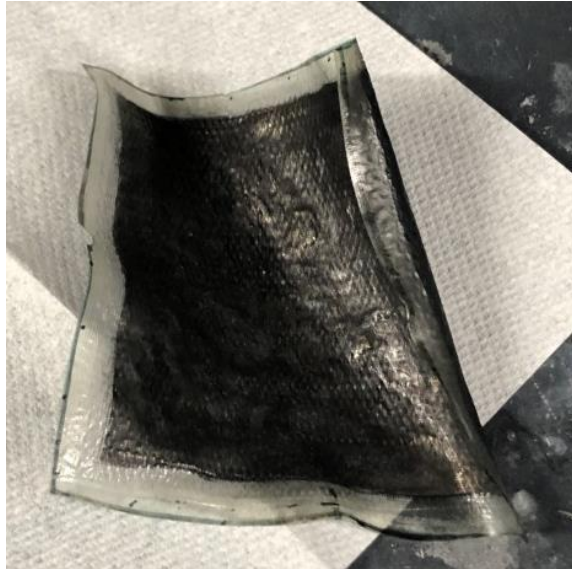
Figure 5.6. Dried out Nafion CCM following experimentation

- Contamination - Patrick Emerick pointed out that outside of the Nafion CCM having likely dried up at points, was also likely exposed to external contamination [28]. This was indicated by reflective spotting only noticeable when held at an angle next to a light source. This external contamination, likely from oxidized titanium mesh or the oxidized bolts clamping the cell together drastically hinders the proton exchange across the membrane, rendering much of the catalyst useless.

- Thick Silicon Rings - Another possible problem with the system was that the silicon rings were just slightly too thick. Similarly to the problem with the area available for the Ultem spacers, this additional thickness may have introduced additional unequal compression

problems. Thinner silicon material is very expensive relative to the allotted MQP budget which is why a better version could not be acquired.

- Degraded O-rings - On the outside of either electrode, there are four O-rings that were used to seal the liquid and gas flow into the backplates. While this was not a problem initially and not one that caused issues with the cell potential/current density data, it did affect the overall mass balance simply because it allowed for water leakage. This problem likely could have been solved by tightening the cell more, however this ran the risk of further damaging the MEA.

All of these issues, while individually not major pieces to worry about, when combined all together, could have culminated into the main reason that the experimental cell experienced such inefficiencies [28]. Furthermore, this clearly indicates the sensitive nature of these cells and that even the slightest disturbances can inflict problems that ultimately result in less effective hydrogen and oxygen production.

6. Design Specifications & Feasibility

6.1 Design Specifications

6.1.1 Mobile Prototype

The final OxyGen product aims to assist users during motionless states or to supplement minute exercise with 40% oxygen intake, compared to 21% with ambient air. During these operations, the average human intakes 6-10 liters of air every minute [29]. Using the model created describing the mass transfer and polarization of a single cell with an active area of 50 cm^2, the operating parameters will be determined to supply the needed oxygen consumption for the user.

A 100 cm^2 cell will be used for the final proposed product. To determine the power supply and the number of cells stacked in series needed, Figure 5.1 was examined to find the polarization requirements for a given flow intake. The system will operate with 4 L/min of air intake for a single cell, translating to the polarization for 2 L/min of air intake for a 50 cm^2 cell. To obtain the greatest current density supplied to the cell for the minimum voltage, the system will be operating as close to the transition point as it can within reasonable limits (95% of the transition point current density). From Figure 5.1, this point was deemed as a current density of 0.435 A/cm^2 having a voltage of 0.91 V. Using equation 3.37, these parameters will give the molar flow rate of oxygen produced at the anode that will be used for consumption. From appendix B, a single cell can produce 0.006763 mol/min of oxygen by supplying 4 L/min of ambient air into the cathode. Deciding the number of cells needed for the system is strictly dependent on the amount of pure oxygen needed to supply ambient air being consumed at 10 liters per minute to reach 40% oxygen. From appendix B, the system will need to supply a steady molar flow rate of 0.0848 mol/min of

pure oxygen to the user. A single cell output will need to be multiplied up to meet supply needs, ultimately meaning that 13 cells in the system with an ambient air intake of 52 L/min, and easily supported by a computer cooling fan was used [30]. 12 V from an external source will need to be supplied to the system to obtain the current density needed for each cell. Using Ohm's Law to calculate the power need for the cell, the following values were determined:

$$P = V * I$$

$$12\ V * 43.5\ A = 522\ W$$

The system, ideally, should be able to operate for most of the day without the need to recharge often, lasting 8 hours. Given this, the battery would be required to have a 350 Ah charge life able to supply 12 V. Advancements in lithium ion battery packs meet the needs of our prototype given the ability to travel and walk around with ease. Being the heaviest part of the assembly, these battery packs weigh around 20 pounds and can last 8 hours of constant operation given our operating parameters [31].

Table 6.1. Design Specifications for Mobile Design

OxyGen® Design Specifications Mobile Design	
Ambient Air Intake	52 L/min
Voltage	12 V
Current	43.5 Amps
Power	522 W
Cells	13
Oxygen Production	6-10 L/min
Oxygen Purity	40%
Battery Operations	6 kWh 350 Ah

6.1.2 Stationary Respirator

Another model prototype is proposed as a stationary respirator used either in hospitals or installed in homes to supplement patients needing 90%> oxygen concentration at 10 L/min. The polarization operations of each cell including the ambient air flow rate will remain the same as the mobile model. Supplying the cells with 4 L/min of ambient air allows each cell to supply 0.006763 mol/min of oxygen. Appendix B calculates that the system will need to supplement 0.3080 mol/min of oxygen to satisfy the needs of the patient. 46 cells are needed to accommodate the molar flow and composition of oxygen intake. 42 V is needed to produce 43.5 A of current for each cell, and a flow of 168 L/min of air is needed to be supplied to the cell. The prototype will be powered by grid electricity directly and will not require a battery to operate.

Using Ohm's Law, the power needed for the design is found to be:

$$P = V * I$$

$$42\ V * 43.5\ A = 1.83\ kW$$

Table 6.2. Design Specifications for Stationary Prototype

OxyGen® Design Specifications Stationary Design	
Ambient air intake	168 L/min
Voltage	42 V
Current	43.5 Amp
Power	1.83 kW
Oxygen Production	6-10 L/min
Oxygen Purity	90%

6.2 Comparison to PSA Unit

Taking the design specifications for the oxygen air purification device into consideration, it is worth comparing these results to those of a pressure swing absorption device, which is currently the more commonly used method of providing patients with oxygen using oxygen concentration. PSAs can provide a continuous flow of concentrated oxygen up to a maximum concentration of 92-95% from room air through one or more oxygen outlets. The most common flow rates provided are around 5-10 liters per minute [32]. PSA's typically consist of an air compressor, dryer, filters, dual separation chambers, and controls, and allow for flow to be divided for at least two pediatric patients with build in flowmeters that allow for continuous flow rate control [32]. The general power efficiency for PSA's is about 70 W/L/min, the general noise level is about 60 dB(A), and the general weight is approximately 27 kg or about 60 pounds [32]. PSAs also require continuous, uninterrupted power, a backup cylinder supply, and continuous maintenance through cleaning of filters and the device exterior, measuring of the operating pressure with the pressure test gauge, measuring of the oxygen concentration with a calibrated oxygen analyzer, testing of power failure alarms, repairing of internal components and maintenance of a spare-parts inventory. The systems have a lifespan of approximately 10 years, are able to measure the oxygen concentration with +/- 1% accuracy, and are able to supply oxygen continuously from temperatures ranging from 10 to 40 degrees Celsius [32]. Finally, as for power requirements, PSA concentrators require continuous AC power ranging anywhere from 110 to 220 Volts [32].

One of the more popularly used brands of devices utilizing PSA technology is Philips Respironics' oxygen concentrators. Looking at the design specifications for Philips' Everflo Oxygen Concentrator allows for some direct comparisons to be made to the Oxygen device. The Everflo

device requires an input voltage of 120V as opposed to the 42V requirement of the OxyGen stationary design, has an input frequency of 60hz, and produces oxygen at a concentration of 93%. While this model is able to produce high purity oxygen, it is worth noting that the OxyGen is device is able to produce almost completely pure oxygen (98% or higher). Additionally, the oxygen produced by both of the proposed models is humidified due to the small amounts of water vapor in the stream following electrolysis. This means that the oxygen will be easier for patients to breathe in than the dry oxygen streams supplied by oxygen concentrators. In terms of size and weight, this model is relatively small and lightweight for a PSA system, weighing in at 31 pounds with dimensions of 15 by 9.5 by 23 inches, which is similar to the estimated 30 pound weight of the Oxygen system. While the system is relatively lightweight for an oxygen concentrator, the amount of oxygen it can produce is on the lower side ranging from only 0.5 to 5 liters per minute as opposed to the 6-10 liters per minute of the OxyGen system. A separate Phillips' model, the Millennium M10 Oxygen Concentrator, can produce up to 10 liters per minute of oxygen. As a result of the higher oxygen production rates though, the weight of the system is much higher at 53 pounds and the voltage required is much higher at 200V. Comparing this to the OxyGen device, the weight is almost twice that of the estimated 30 pounds for the proposed model, and the voltage is about 4 times higher than the 52V of the stationary model. Phillips also produces portable models that are much more lightweight, with the SimplyGo model weighing in at 10 pounds. As a result of the smaller system though, the device is only able to produce oxygen at a maximum flow rate of 2 liters per minute or pulse doses of up to 72 milliliters as opposed to the OxyGen device, which can still produce 6 to 10 liters per minute in its mobile design. It also only has a maximum battery life of 2 to 3 hours. While the proposed design for the mobile model of the OxyGen device has an

8 hour battery life, it could also be reduced to a 2 hour battery life the same as the Philips device, resulting in a much smaller battery required and a similar weight between both devices. The main comparisons made from the PSA devices specifications to those of the OxyGen device are differences in size, weight, power requirements and oxygen produced. PSA condensers producing higher flow rates of oxygen potentially weigh up to 50 to 60 pounds, which is about twice the weight of the proposed design for the OxyGen device. Additionally, the overall power requirement of the proposed oxygen purification device is significantly lower than that of general PSA systems, which require three to five times as much voltage as the OxyGen device in its stationary design or more than ten times as much voltage as the OxyGen device in its mobile design. The rate of oxygen production for the OxyGen system is in the range of 6 to 10 liters per minute. The only PSA concentrators able to reach these flow rates are the higher costing, stationary models. Smaller or portable concentrators are generally unable to achieve oxygen flow rates of more than 5 liters per minute. While PSA concentrators can produce Oxygen with high purity, the OxyGen is able to produce essentially completely pure oxygen that is also humidified, making it much easier to breathe than just dry oxygen. General less quantitative differences between the two devices worth noting include the maintenance required, the portability of the devices, the general costs associated with each. PSA devices require a significant amount of maintenance in comparison to the OxyGen device due to necessary filter cleaning, pressure regulation, testing of power failure alarms and repairing of internal mechanisms. The OxyGen device will likely need occasional repairing and cleaning, but not to the same extent as the PSA device due to the difference in the number of internal components and size. Additionally, due to the size required to achieve high flow rates of oxygen from PSA concentrators, portable PSA devices are not much of an option for patients who

need higher quantities of oxygen as opposed to the OxyGen device of which specifications of a mobile design able to produce 6-10 liters per minute of oxygen have already been proposed. Finally, while the overall cost of each device remains relatively low, the requirement of spare parts as well as constant maintenance and potential repairs for the PSA design will likely push it to become more expensive in the long run.

7. Conclusions

To advance the development of oxygen therapy for the millions of users around the globe who rely on the practice, OxyGen is proposed as an alternative solution to help patients receive purified hydrated oxygen with ease. Proton exchange membrane (PEM) technology and theory was used to manipulate a PEM water electrolyzer to produce high purity hydrated oxygen with reduced power usage by feeding air into the cathode, decreasing the needed potential to produce oxygen through the oxygen evolution reaction (OER). At the same time, this depletes the hydrogen production in the oxygen reduction reaction (ORR) at the cathode, making the process safer for the user as hydrogen can be dangerous. This process requires little maintenance as the water would be recycled from the cathode to the anode, creating a closed loop, meaning the only external supply for the system would be ambient air provided by a fan and an external power source.

Derived from a modified Butler-Volmer equation along with mass action and other chemical and physical principles, a model describing the polarization of the system was created to predict how a single cell may operate under any prescribed conditions. Experimental trials of a cell were conducted to test the feasibility of the design and see how the model would hold up against collected data. Unfortunately, there were no successful experiments due to many possible errors and literature data needed to be used. The model was backed by experimental data produced by CSIRO Energy Technology through polarization plots under the same conditions. Higher and lower current densities were closer to identical, but as predicted in deriving the equation, the transition point is not well described in the model. In practice, there is a more gradual transition between the two reactions occurring on the cathode, the ORR and HER, but in predicting the behavior, it was assumed that the reactions would occur independently.

Two proposed prototypes of the OxyGen system were made using predicted operating conditions of a single cell and then built up to meet production needs. A mobile model would allow users to move around with ease and create a more comfortable environment for them compared to traditional methods of oxygen therapy. It is designed to produce between 6-10 L/min of hydrated oxygen of 40% purity requiring 522 W of power with 13 cells. This can be powered by a computer cooling fan to supply the ambient air and a 12 V lithium-ion battery with a 12-hour battery life. This system will weigh approximately 30 pounds and can be worn as either a backpack or a sling. For more serious cases, a stationary respirator was also proposed to deliver 90% pure hydrated oxygen at 6-10 L/min. This can be installed in most homes and hospitals. It requires 42 V and 1.8 kW of power with 42 operating cells. It will require a slightly larger fan compared to the mobile model because there are more than three times the amount of cells. Comparing these specifications to those of the more common means of oxygen production currently, pressure swing absorption condensers or PSA's, the most notable differences consist of the size, mobility, oxygen flow rates, and the voltage required. PSA's require voltages ranging from 110 to 220 volts, approximately three to ten times more than the voltage requirements of the OxyGen system depending on the mode and weigh 50 to 60 pounds on average for devices that can produce up to 10 liters per minute, about twice as much as the OxyGen system. While both systems can produce oxygen at 6-10 liters per minute, PSA systems can only do so in heavy weight, stationary models. Lighter and mobile PSA models produce oxygen at much more limited flow rates. Finally, it is also worth noting that, due to the few parts necessary in the OxyGen system, it requires significantly less maintenance and cleaning than PSA's and can be moved around much easier while still producing higher oxygen flow rates.

7.1 Experimental Recommendations

Given the lack of success previously discussed surrounding the experimentation of the electrolyzer, a few recommendations have been identified for the physical continuation of this project. For one, it is highly recommended that a 5-layer MEA be purchased instead of a CCM and individual GDL's for either side. Not only would it make assembly of the cell much simpler, but it would also help to ensure that the membrane does not become deformed or contaminated due to the rigidity of a metallic GDL which many contain. Purchase of a full MEA would also eliminate the potential problems of not having an MPL as they are usually part of these pre-assembled systems. Secondly, either a new electrolyzer unit as a whole or at the bare minimum, the bipolar plates and electrodes for this unit must be replaced. As previously mentioned, the current graphite bipolar plates at one point were believed to have been used with aggressively corrosive chemicals. Similarly, as previously discussed, the gold plating on each electrode has come off making them fewer effective conductors. Replacing these, or the cell as a whole would hopefully eliminate these problems entirely. Given that these components are quite expensive for the experimental scale of a 50 cm^2 active area, searching for outside funding ventures such as WPI's Tinkerbox grant or others like this would help ease this problem. Lastly, when it comes to designing the cell, purchase, and assembly, it is highly recommended that a local expert, such as Patrick Emerick, be brought in to provide his feedback and aid in the process.

7.2 Modeling Recommendations

Although the model was able to predict the polarization of the OxyGen cell at 80°C for six different flow rates between 0-2 L/min accurately for lower and high current densities, there are elements of the model which can be further improved upon. As mentioned before, the model created is not able to predict the polarization of the cell during the transition point. Although time restricted further analysis and improvements of the model, the next step that should be taken is to establish a reason for a more gradual increase in polarization from OxyGen operations to PEM-WE polarization instead of an abrupt switch at the limiting current density.

Once experimental collection for various flow rates at different temperatures and possibly different pressures in the electrode chambers, the model should then be compared at the varying operating parameters to see how it holds up against any conditions. This would further prove the validity of the model, especially at lower and higher current densities. The model would then be able to theoretically optimize the operating conditions of the system in seconds to determine how experiments should be completed.

8. References

1.   Wood, L. *Worldwide Portable Oxygen Concentrators Market (2020-2026) - Shares, Strategy, and Forecasts*. 2020   October 6, 2020]; Available from: https://www.businesswire.com/news/home/20200501005439/en/Worldwide-Portable-Oxygen-Concentrators-Market-2020-to-2026---Shares-Strategy-and-Forecasts---ResearchAndMarkets.com.

2.   *COVID 19 and the Oxygen Bottleneck*, in *Bulletin of the World Health Organization*. 2020, World Health Organization. p. 586-587.

3.   Jacobs, S., et al., *Optimizing Home Oxygen Therapy*. 2018, American Thoriac Society Workshop.

4.   Raman, G., et al., *A Horizon Scan: Uses of Hyperbaric Oxygen Therapy*. 2006.

5.   Rao, P. and M. Muller, *Industrial Oxygen: Its Generation and Use*. 2007, Rutgers University.

6.   *Types of Fuel Cells*. 2020   October 16, 2020]; Available from: https://www.energy.gov/eere/fuelcells/types-fuel-cells.

7.   Salva, J., et al., *Optimization of a PEM Fuel Cell Operating Conditions: Obtaining the Maximum Performance Polarization Curve*. International Journal of Hydrogen Energy, 2016. **41**(43): p. 19713-19723.

8.   Datta, R., *Chapter 5: The Basic Fuel Cell Model*. Worcester Polytechnic Institute. p. 323-393.

9.   Wang, H. and H. Abruna, *IrPdRu/C as H2 Oxidation Catalysts for Alkaline Fuel Cells*. Journal of the American Chemical Society, 2017. **139**(20): p. 6807-6810.

10.   Vuppala, R., et al., *Optimization of Membrane Electrode Assembly of PEM Fuel Cell by Response Surface Method*. Molecules, 2019. **24**(17).

11.   Datta, R., et al., *PEM Electrolysis for Hydrogen Production: Principles and Applications*. 1st ed. 2016: Taylor & Francis Group.

12.   Satyapal, S. *Hydrogen: A Clean, Flexible Energy Carrier*. 2017   October 16, 2020]; Available from: https://www.energy.gov/eere/articles/hydrogen-clean-flexible-energy-carrier.

13.   *Hydrogen explained: Production of Hydrogen*. 2020 October 16, 2020]; Available from: https://www.eia.gov/energyexplained/hydrogen/production-of-hydrogen.php.

14.   Kumar, S. and V. Himabindu, *Hydrogen Production by PEM Water Electrolysis - A Review*. Materials Science for Energy Technologies, 2019. **2**(3): p. 442-454.

15.   Datta, R., *Chapter 6: PEM Water Electrolyzer*. Worcester Polytechnic Institute. p. 395-436.

16.   Giddey, S., F.T. Ciacchi, and S. Badwal, *High Purity Oxygen Production with a Polymer Electrolyte Membrane Electrolyser*. Journal of Membrane Science, 2010. **346**(1): p. 227-232.

17.   Sartory, M., et al., *Theoretical and Experimental Analysis of an Asymmetric High Pressure PEM Water Electrolyser up to 155 bar*. International Journal of Hydrogen Energy, 2017. **42**(52).

18.   Stein, T. and Y. Ein-Eli, *Proton Exchange Membrane (PEM) Fuel Cell Bipolar Plates Prepared from a Physical Vapor Deposition (PVD) Titanium nitride (TiN) Coated AISI416 Stainless-steel.* SN Applied Sciences, 2019. **1**.

19.   Spiegel, C. *Fuel Cell Vehicles - Automobiles*. 2019 October 16, 2020]; Available from: https://www.fuelcellstore.com/blog-section/fuel-cell-vehicles-automobiles.

20.   *Fuel Cell Graphite Bipolar Plates*. Alibaba.com.

21.   Nagamoto, H., *Fuel Cells: Electrochemical Reactions*, in *Encyclopedia of Materials: Science and Technology*. 2001. p. 3359-3367.

22.   Yan, Q., H. Toghiani, and H. Causey, *Steady state and dynamic performance of proton exchange membrane fuel cells (PEMFCs) under various operating conditions and load changes.* Journal of Power Sources, 2006. **161**(1): p. 492-502.

23.   *Water*.   2018   October   16,   2020];   Available   from: https://webbook.nist.gov/cgi/cbook.cgi?ID=C7732185&Mask=4&Type=ANTOINE&Plot=on.

24.   Tafoli-Masoule, M., M. Shakeri, and A. Bahrami, *Process parameters for maximum power of a proton exchange membrane fuel cell.* Journal of Petroleum and Gas Engineering, 2012. **3**(2): p. 16-25.

25.   Barbir, F., *PEM Fuel Cells*. 2nd ed. 2012: Elsevier Inc.

26.   Kalinnikov, A., et al., *Study of the Electrochemical Oxygen Pump Based on Solid Polymer Electrolyte.* Russian Journal of Applied Chemistry, 2018. **91**: p. 927-929.

27.   Sunden, B., *Hydrogen, Batteries and Fuel Cells*. 2019.

28.   Emerick, P., *OxyGen Experimentation Diagnosis Interview*, C. Buek, Editor. 2021.

29.   Miller, K. *Oxygen Administration: What Is the Best Choice?* 2015.

30.   *Cooling   Your   Computer*.   2019   [cited   2021;   Available   from: www.skillbank.co.uk/cooling.html#:~:text=A%20typical%20120mm%20fan%20will,power%20rating%20and%20fan%20size.

31.   *500Ah 12V LiFePO4 Heated Battery Kit - 5 Batteris*. Available from: battlebornbatteries.com/product/500ah-12v-lifepo4-heated-battery-kit-5-batteries/.

32.   Organization, W.H., *WHO-UNICEF Technical Specifications and Guidance For Oxygen Therapy Devices*. 2019. p. 164.

9. Appendices

Appendix A - OxyGen Modeling Parameters

Table A.1 OxyGen Pump Modeling ORR Parameters

ORR Parameters			
R	J/molK	Gas Constant	8.3145
T	K	Temperature	353
To	K	Standard Temperature	298.15
B	-	Symetry Factory	0.5
Nu	-	Electron Reaction Coefficeint	2
F	s*A/mol	Faraday's Constant	96485
Φ^0_o	V	Standard Equilibrium Electrode Potential	1.229
Φ_o	V	Equilibrium Elecrode Potential	1.202
i_x	A/cm2	Crossover Current Density	0
i^*_0	A/cm2	Exchange Current Desnity	5×10^{-8}
$i^*_{0,o}$	A/cm2	Standard Exchange Current Desnity	1×10^{-10}
γ	cm^2Pt/cm^2MEA	Roughness Factor	250
E	kJ/mol	Activation Energy	285.82
P_{total}	atm	Pressure of Electrode	1
P_{H2O}	atm	Partial Pressure of Water Vapor	0.467
ΔG^o	J/mol	Free Gibbs Energy	-237.2
ΔH^o	J/mol	Change in Enthalpy	-285.8
ΔS^o	J/molK	Change in Entropy	188.7
P	$kg\ s^{-1}m^{-2}Pa^{-1}$	Permeance	0.1619
v_o	L/min	Air Flow Rate	0-2

Table A.2 OxyGen Pump Modeling OER Parameters

OER Parameters			
R	J/molK	Gas Constant	8.3145
T	K	Temperature	353
To	K	Standard Temperature	298.15
B	-	Symetry Factory	0.5
Nu	-	Electron Reaction Coefficeint	3
F	s*A/mol	Faraday's Constant	96485
Φ^0_o	V	Standard Equilibrium Electrode Potential	1.229
Φ_o	V	Equilibrium Elecrode Potential	1.202
i_x	A/cm^2	Crossover Current Density	0
$i^*_{0,o}$	A/cm^2	Exchange Current Desnity	5×10^{-10}
i^*	A/cm^2	Standard Exchange Current Desnity	1×10^{-12}
i_L	A/cm^2		10
γ	cm2Pt/cm2MEA	Roughness Factor	100
E	kJ/mol	Activation Energy	285.82
p_{total}	atm	Pressure of Electrode	1
p_{H2O}	atm	Partial Pressure of Water Vapor	0.467
ΔG^o	J/mol	Free Gibbs Energy	237.2
ΔH^o	J/mol	Change in Enthalpy	285.8
ΔS^o	J/molK	Change in Entropy	-188.7

Table A.3 OxyGen Pump Modeling HER Parameters

HER Parameters			
R	J/molK	Gas Constant	8.3145
T	K	Temperature	353
To	K	Standard Temperature	298.15
B	-	Symetry Factory	0.5
Nu	-	Electron Reaction Coefficeint	4
F	s*A/mol	Faraday's Constant	96485
Φ^0_a	V	Standard Equilibrium Electrode Potential	1.229
Φ_a	V	Equilibrium Elecrode Potential	1.202
i_x	A/cm^2	Crossover Current Density	0
$i^*_{0,a}$	A/cm^2	Exchange Current Desnity	5×10^{-2}
i^*	A/cm^2	Standard Exchange Current Desnity	1×10^{-3}
i_L	A/cm^2		10
γ	cm2Pt/cm2MEA	Roughness Factor	175
P_{total}	atm	Pressure of Electrode	1
P_{H2O}	atm	Partial Pressure of Water Vapor	0.467
ΔG^o	J/mol	Free Gibbs Energy	0
ΔH^o	J/mol	Change in Enthalpy	0
ΔS^o	J/molK	Change in Entropy	130.6

Table A.4 OxyGen Pump Modeling Membrane Parameters

Membrane Parameters			
σ	S/cm^2	Conductivity	1×10^{-3}
L_B	cm	Membrane Thickness	175×10^{-4}

Appendix B - Design Spec. Calculations

Single Cell Production

Voltage for each cell: 0.91 V

Current for each cell: $0.435A/cm^2 * 100cm^2 = 43.5$ A

Molar flow of oxygen produced in the anode for a single cell

$$n_{+,O_2,out} = \frac{43.5\ A}{|4| * 96485\ \frac{C}{mol}}$$

$$n_{+,O_2,out} = 0.0001271\ \frac{mol}{s} = 0.006763\ \frac{mol}{min}$$

Mobile Prototype Oxygen Production

User needs 10 liters/min of air containing 40% oxygen

Assuming ideal gas:

$$10\ \frac{L\ air}{min}\ /\ 22.4\ \frac{L}{mol} = 0.4464\ \frac{mol\ air}{min}$$

Oxygen will make up 40% of air intake:

$$0.4464\ \frac{mol\ air}{min} * \frac{0.40\ mol\ O2}{1\ mol\ air} = 0.1786\ \frac{mol\ O2}{min}$$

Amount of oxygen supplied from ambient air:

$$0.4464\ \frac{mol\ air}{min} * \frac{0.21\ mol\ O2}{1\ mol\ air} = 0.09375\ \frac{mol\ O2}{min}$$

Amount of pure oxygen that needs to be produced to satisfy user:

$$0.1786\ \frac{mol\ O2}{min} = 0.09375\ \frac{mol\ O2}{min} + nO_{2,OxyGen}$$

$$nO_{2,OxyGen} = 0.08481\frac{mol}{min}$$

Stationary Respirator Oxygen Production

User needs 10 liters/min of air containing 90% oxygen

Oxygen will make up 90% of air intake:

$$0.4464 \; \frac{mol \; air}{min} * \frac{0.9 \; mol \; O2}{1 \; mol \; air} = 0.40176 \; \frac{mol \; O2}{min}$$

Amount of pure oxygen that needs to be produced to satisfy user:

$$0.40176 \; \frac{mol \; O2}{min} = 0.09375 \; \frac{mol \; O2}{min} + nO_{2,OxyGen}$$

$$nO_{2,OxyGen} = 0.3080 \; \frac{mol}{min}$$